NASA/TM-20230010620

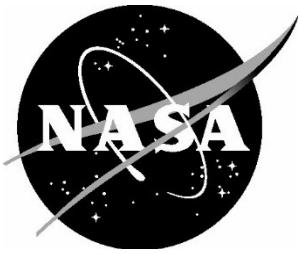

Development of a Field-Deployable Microphone Phased Array for Airframe Noise Flyover Measurements

William M. Humphreys, Jr., David P. Lockard, Mehdi R. Khorrami,
William G. Culliton, Robert G. McSwain, and Chester V. Dolph
Langley Research Center, Hampton, Virginia

Patricio A. Ravetta
AVEC, Inc., Blacksburg, Virginia

National Aeronautics and
Space Administration

Langley Research Center
Hampton, Virginia 23681-2199

August 2023

NASA STI Program . . . in Profile

Since its founding, NASA has been dedicated to the advancement of aeronautics and space science. The NASA scientific and technical information (STI) program plays a key part in helping NASA maintain this important role.

The NASA STI program operates under the auspices of the Agency Chief Information Officer. It collects, organizes, provides for archiving, and disseminates NASA's STI. The NASA STI program provides access to the NASA Aeronautics and Space Database and its public interface, the NASA Technical Report Server, thus providing one of the largest collections of aeronautical and space science STI in the world. Results are published in both non-NASA channels and by NASA in the NASA STI Report Series, which includes the following report types:

- TECHNICAL PUBLICATION. Reports of completed research or a major significant phase of research that present the results of NASA programs and include extensive data or theoretical analysis. Includes compilations of significant scientific and technical data and information deemed to be of continuing reference value. NASA counterpart of peer-reviewed formal professional papers, but having less stringent limitations on manuscript length and extent of graphic presentations.

- TECHNICAL MEMORANDUM. Scientific and technical findings that are preliminary or of specialized interest, e.g., quick release reports, working papers, and bibliographies that contain minimal annotation. Does not contain extensive analysis.

- CONTRACTOR REPORT. Scientific and technical findings by NASA-sponsored contractors and grantees.

- CONFERENCE PUBLICATION. Collected papers from scientific and technical conferences, symposia, seminars, or other meetings sponsored or co-sponsored by NASA.

- SPECIAL PUBLICATION. Scientific, technical, or historical information from NASA programs, projects, and missions, often concerned with subjects having substantial public interest.

- TECHNICAL TRANSLATION. English-language translations of foreign scientific and technical material pertinent to NASA's mission.

Specialized services also include creating custom thesauri, building customized databases, and organizing and publishing research results.

For more information about the NASA STI program, see the following:

- Access the NASA STI program home page at *http://www.sti.nasa.gov*

- E-mail your question via the Internet to help@sti.nasa.gov

- Fax your question to the NASA STI Help Desk at 443-757-5803

- Phone the NASA STI Help Desk at 443-757-5802

- Write to:
  NASA STI Help Desk
  NASA Center for AeroSpace Information
  7115 Standard Drive
  Hanover, MD 21076-1320

NASA/TM-20230010620

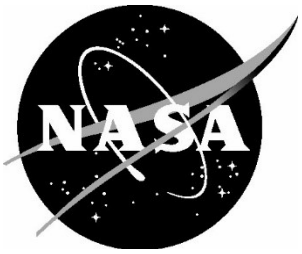

Development of a Field-Deployable Microphone Phased Array for Airframe Noise Flyover Measurements

William M. Humphreys, Jr., David P. Lockard, Mehdi R. Khorrami,
William G. Culliton, Robert G. McSwain, and Chester V. Dolph
Langley Research Center, Hampton, Virginia

Patricio A. Ravetta
AVEC, Inc., Blacksburg, Virginia

National Aeronautics and
Space Administration

Langley Research Center
Hampton, Virginia 23681-2199

August 2023

Available from:

NASA STI Program / Mail Stop 148
NASA Langley Research Center
Hampton, VA 23681-2199
Fax: 757-864-6500

Acronyms

ACV	Acoustic Calibration Vehicle
ADL	Acoustic Development Laboratory
AFB	Air Force Base
AGL	Above Ground Level
ARM	Acoustic Research Measurements
CLEAN-SC	CLEAN Deconvolution Algorithm Based on Source Coherence
DAMAS	Deconvolution Approach for the Mapping of Acoustic Sources
EPNL	Effective Perceived Noise Level
ERA	Environmentally Responsible Aviation
FDC	Flight Demonstrations and Capabilities
IEPE	Integrated Electronics Piezo-Electric
IRIG-B	Inter-range Instrumentation Group Time Code B
LaRC	NASA Langley Research Center
NAS	Network-attached Storage
PCB	Printed Circuit Board
PCIe	Peripheral Component Interconnect Express
SALT	Structural Acoustic Loads Transmission
SPL	Sound Pressure Level
SSD	Solid State Drive
sUAS	Small Uncrewed Aerial System
THD	Total Harmonic Distortion, percent
UTC	Universal Time Code, seconds since midnight
WFF	Wallops Flight Facility

Nomenclature

A_i	Amplitude of i^{th} harmonic for THD computation, volts
$C(t)$	Convective amplification
d	Line-of-sight distance from ACV to microphone, feet
D_f	Doppler frequency shift, dimensionless ($= f_m/f_r$)
f	Frequency, Hertz
f_m	Moving Doppler frequency, Hertz
f_r	Reference (motionless) Doppler frequency, Hertz
h	Height of atmospheric attenuation layer, feet
H_i	Average humidity across i^{th} atmospheric layer, percent
i	Index number (microphones and atmospheric layers)
M	Mach number
$p_i(t)$	Pressure Recorded at Microphone i
P_θ	Polar directivity function
P_φ	Azimuthal directivity function
r	Distance from microphone to location directly under ACV, feet
$r_i(t)$	Time-dependent distance from measurement location to microphone i, feet
t	Time, seconds
T_i	Average temperature across i^{th} atmospheric layer, deg F
α_i	Directivity angle for i^{th} array microphone, degrees
$\Delta t_i(t)$	Sound propagation time for microphone i, seconds
$\theta_e(t)$	Time-dependent emission angle from a source to microphone i, degrees
ξ	Atmospheric attenuation geometric angle to microphone, degrees
ω	Angular frequency

Contents

1.0 Abstract

This technical memorandum describes in detail the construction and use of a large channel-count, field-deployable microphone phased array designed for airframe noise flyover measurements for a range of aircraft types and scales. The array incorporated 185 hardened, weather-resistant sensors suitable for outdoor use. A custom 4-mA current loop receiver circuit with temperature compensation was developed to power the sensors over extended cable lengths with minimal loss of signal-to-noise. Extensive calibrations and performance testing of the sensors were conducted to verify the design specifications. A compact data system combining sensor power, signal conditioning, and digitization was assembled for use with the array. Complementing the data system was a robust analysis system capable of near real-time presentation of beamformed and deconvolved contour plots and integrated spectra obtained from data acquired during flyover passes of the array. Additional instrumentation systems needed to process the array data were also developed, including a commercial 10-meter weather station comprised of a sonic anemometer, aspirated temperature/humidity probe and pressure sensor. Unique methods for assessing the health of the array in-situ were developed and demonstrated. A detailed mock-up of the instrumentation suite (phased array, weather station, and data processor) was performed in the NASA Langley Acoustic Development Laboratory in 2014 to vet the system performance. Issues with the sensors and electronics were identified during the mock-up and subsequently corrected. The array was then deployed for preliminary field testing at Fort A.P. Hill in Virginia in 2015 followed by the array being utilized in three separate full-scale airframe noise test campaigns at Edwards Air Force Base in California from 2016 to 2018 where the system was used to characterize the noise generated by both baseline and treated flaps and main landing gear on a commercial transport-sized vehicle.

2.0 Introduction

NASA has funded a number of projects over the past decade formulated to explore vehicle concepts and technologies that are designed to improve fuel efficiency, reduce noise levels, and decrease harmful emissions for both the current and future fleet of aircraft. These projects include the now completed Environmentally Responsible Aviation (ERA) Project [1] and its follow-on, the Flight Demonstrations and Capabilities (FDC) Project. In particular, the FDC Project promotes focused flight experiments to validate critical technologies, including noise reduction concepts [2]. These flight experiments require the use of measurement diagnostics, both aircraft- and ground-based, in order to quantitatively evaluate the benefits of specific noise treatments and mitigation concepts as applied to aircraft high-lift (i.e., leading edge slats and trailing edge flaps) and undercarriage (i.e., landing gear) structures. In the realm of noise reduction characterization, one of the primary tools for such quantitative measurements is the microphone phased array.

Modern phased arrays for aeroacoustic research have as their origin early radio and radar antenna arrays and U.S. Navy hydrophone arrays (used for the detection of submarines as early as World War II) [3 – 4]. Soderman and Noble were among the first researchers to adapt this earlier work for aeroacoustics when they constructed a one-dimensional end-fire array to evaluate jet noise in the NASA Ames 40- by 80-foot Wind Tunnel [5 – 6]. At the same time, Billingsley and Kinns constructed a one-dimensional linear array of microphones for real-time sound source location on full-size jet engines [7]. These early one-dimensional arrays were extended to include two-dimensional microphone layouts with the work of Brooks, Marcolini and Pope [8 – 9], Underbrink and Dougherty [10], Mosher and Watts [11 – 12], and Humphreys et al. [13]. Along with the development of multi-dimensional arrays, robust acoustic processing and imaging algorithms and techniques have been developed over the past two decades, starting with conventional delay and sum beamforming in the time and frequency domains [14]. These early techniques were augmented or in some cases supplanted by more advanced source localization algorithms including point spread function deconvolution [15 – 16] and, most recently, generalized inverse methods [17] and functional beamforming [18]. An extensive review of processing and imaging methods using phased arrays is given by Merino-Martinez et al. [19]. A review of various array patterns and design methodologies is given by Underbrink [20 – 21].

While traditionally phased arrays have been utilized in ground test facilities (e.g., wind tunnels) to obtain noise location and strength measurements on various model geometries, there has been an increasing need to use these arrays in outdoor environments for flyover noise measurements. Early work in the use of outdoor arrays for airframe and propulsive noise measurements was pioneered by Michel et al. [22 – 23], Ulf et al. [24], and Piet et al. [25 – 26]. Boeing Commercial Airplanes has extensively used high-channel count phased arrays for routine certification and testing of aircraft [27]. An overview of various array geometries and designs for flyover testing is summarized by Brusniak et al. [28].

NASA Langley Research Center (LaRC) undertook the development of phased array field systems starting in 2005 to provide an in-house capability for conducting flyover measurement campaigns to characterize airframe and propulsion noise on full-scale aircraft. This technical memorandum describes in detail the design, construction and use of one such large channel-count, field-deployable microphone array system that has been field tested and validated in a number of test campaigns. The development of the sensors for the array along with methods for characterizing their performance are described. Additionally, methods for processing the microphone data and for assessing the health of the array during long-duration deployments are described.

This report is organized with a background on Langley-deployed field arrays presented in Section 3, followed by technical details on the novel array construction presented in Section 4. Laboratory characterization and calibration of the array sensors is presented in Section 5. Mockup testing of the array is presented in Section 6, followed by descriptions of preliminary field testing and production use of the array in Sections 7 and 8. Finally, novel array health monitoring methods and procedures are described in detail in Section 9 followed by some lessons learned in Section 10.

3.0 Historical Field Array Measurement Capabilities

NASA Langley has a long history of successfully utilizing microphone arrays in both ground test facilities (i.e., wind tunnels) and for aircraft flyover testing. Regarding the latter, this section describes two legacy field deployments performed in 2005 and 2006 utilizing an initial-generation hardware system at the NASA Wallops Flight Facility (WFF).

3.1 Wallops Flight Facility Array - 2005

A risk reduction array test was successfully conducted at the WFF in August 2005. The purpose of the test was to demonstrate the capability to make phased array measurements of an aircraft in flight in order to localize and quantify various noise sources on the aircraft. A secondary goal was to identify limitations with the array hardware (originally used for passive wake vortex detection and inherited from the Federal Aviation Administration) in order to resolve any deficiencies prior to conducting extensive production testing using the system.

The array was deployed on the grass overrun area of WFF runway 17 as shown in Figure 1. It utilized 113 low-cost electret microphones arranged in a spiral arm pattern approximately 85 feet in diameter (Figure 2). The inner 41 microphones were placed on a central mounting plate while the remainder of the sensors were deployed on individual ground plates (Figure 3) and covered with small plastic traffic cones for environmental protection when not in use. The data acquisition system was housed in two environmentally controlled cabinets placed at the perimeter of the array (Figure 4). The test aircraft that was flown over the array was a Cirrus SR22 research vehicle with a single variable pitch propeller for propulsion. A total of five test flights were conducted over a 10-day period with a total of 106 aircraft passes completed over the array.

Figure 1. Overrun Area of WFF Runway 17, showing covered array microphones. [Source: NASA]

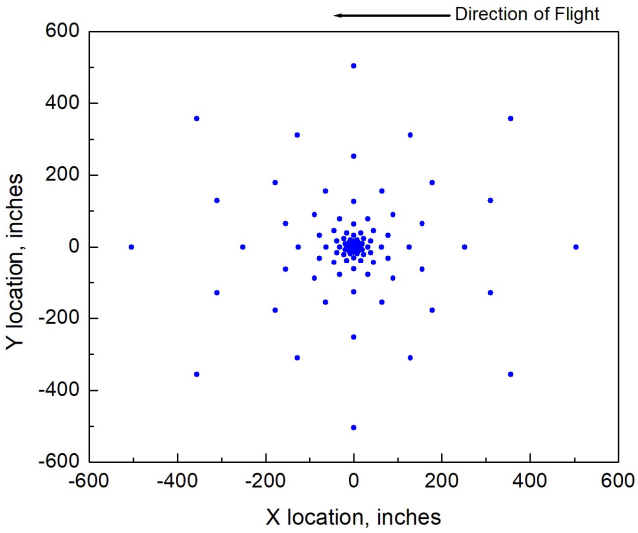

Figure 2. Array pattern deployed at WFF in 2005.

Figure 3. Deployed microphone in 2005. [Source: NASA]

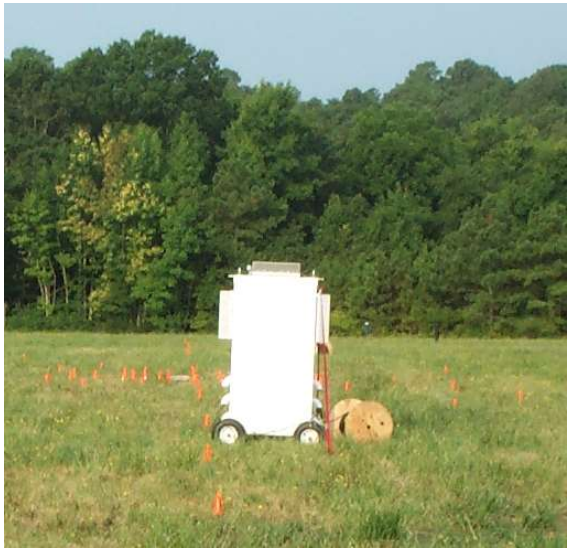

Figure 4. Data acquisition enclosure [Source: NASA]

While in general the array performance was nominal, there were some serious deficiencies noted with the hardware that needed to be addressed:

- The microphones were not hardened against moisture intrusion and several sensors were damaged during heavy rain events at the site, even with the use of traffic cones to protect them.

- The signal conditioners utilized in the data acquisition system were not hardened for use in extreme environmental conditions of high heat and humidity, and thus exhibited intermittent failures during the deployment. The environmental enclosures housing the conditioners were equipped with thermoelectric coolers and fans; however, these were inadequate to properly control the environment within the enclosures.

3.2 Wallops Array – 2006

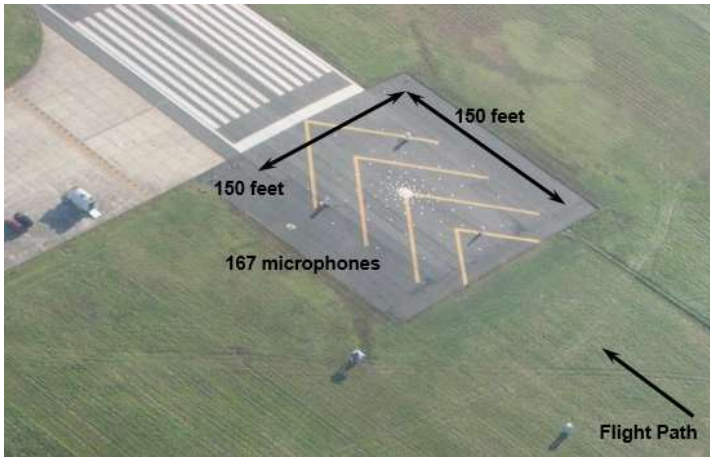

Figure 5. WFF Runway 4 overrun area. [Source: NASA]

Following the risk reduction tests in 2005, a joint NASA-Gulfstream flight test using an enlarged version of the field array was conducted at WFF in October 2006 where Gulfstream G450 and G550 aircraft were flight tested to determine their airframe noise signatures [29]. For this deployment, the array was assembled on the paved overrun area of runway 4 as shown in Figure 5. The number of electret microphones in the array was increased to 167 and the sensors were arranged in a spiral arm pattern approximately 150 feet in diameter (Figure 6). In a similar manner to the 2005 deployment, the inner 49 microphones were mounted on a central plate with the remainder deployed on individual ground plates. Based on lessons learned from the risk reduction tests, new more robust signal conditioners were procured

for the data acquisition system, with the data system housed in three environmentally-controlled enclosures located around the perimeter of the array.

While useful measurements were obtained during the 2006 deployment of the array, there were a number of issues observed with the operational performance of the array:

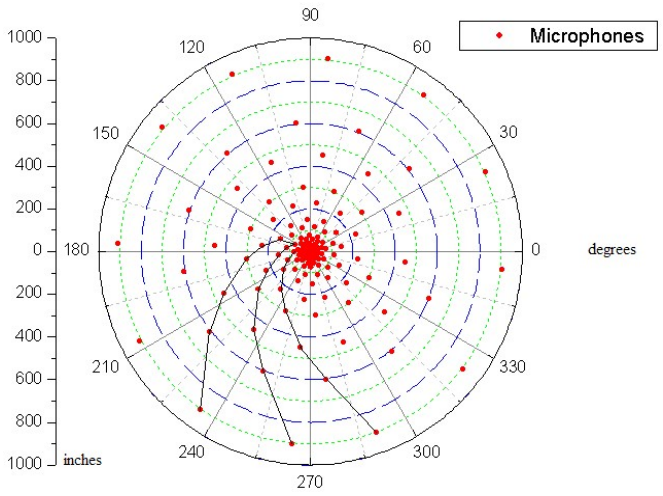

Figure 6. Array pattern deployed at WFF in 2006.

- As with the 2005 deployment, the microphones were not hardened for use in an outdoor environment. Due to moisture contamination, the sensitivity of the sensors drifted significantly during the six-week test campaign, making accurate quantitative measurements of noise levels difficult. Further, there was no effective method for calibrating the entire array of microphones in-situ or for monitoring the health of the array as a function of time.
- The environmental enclosures for the signal conditioning and data acquisition hardware were tall and positioned very close to the perimeter of the array. This provided multiple acoustic scattering and reflecting surfaces inside the aperture of the array, partially degrading the array performance.
- The environmental enclosures incorporated ventilation and thermoelectric air conditioning. However, these systems generated too much noise near the microphones and were ineffective at sufficiently reducing the temperatures inside the enclosures, causing equipment failures during the test campaign.

In order to address the issues observed during the WFF 2005 and 2006 deployments, a completely new array design was developed suitable for long-duration outdoor deployment where airframe and propulsive noise measurements are desired for a range of aircraft types and scales. The new array incorporated 185 hardened, weather-resistant sensors that used custom 4-mA current loop circuits with temperature compensation to power the sensors over extended cable lengths with minimal degradation of the signal to noise ratio and frequency response. Along with the new sensors, a new data system combining sensor power, signal conditioning, and digitization was assembled for use at a central site away from the array to minimize acoustic scattering near the array aperture.

4.0 Microphone Phased Array Details

This section describes the array design in more detail. Section 4.1 addresses the sensors, Section 4.2 describes the data acquisition system, Section 4.3 outlines data reduction methods, and Section 4.4 describes peripheral instrumentation supporting the array.

4.1 Sensors

Microphone Selection: The phased array system utilized 185 custom hardened and weatherproof microphones designed around a commercially available sensor. An ensemble of strict performance requirements was defined for the sensors based on the needs of the aeroacoustic community when performing measurements of airframe noise and propulsion sources in flight. These requirements included a reasonably flat frequency response over a 20 Hz to 10 kHz range, a sensitivity of greater than 2 mV/Pa (i.e., greater than -54 dB with respect to 1 V/Pa), a noise floor less than 40 dBA, and sensors able to survive submersion in 1 inch of water or more (due to the need for extended outdoor placement of the units). After evaluating several commercially available sensors, the Knowles WP-23849 microphone capsule was chosen as the sensing element for the array.* This microphone exhibits a flat frequency response to approximately 8 kHz and is waterproof to 9.8 feet of submersion. Note that since sound waves with frequencies above 6-7 kHz are significantly attenuated during atmospheric propagation and are deemphasized due to application of acoustic A-weighting, the 8-kHz range was deemed to be a reasonable compromise in the requirements.

The Knowles microphone is intrinsically a voltage-driven device. However, due to a requirement to use 400-foot cables to transmit the microphone signals from the array to the central data acquisition system, a custom two-wire, low-noise, 4-mA constant current excitation system was developed to power the sensors. The microphone receiver circuit used to perform this function is shown in Figure 7. The circuit included

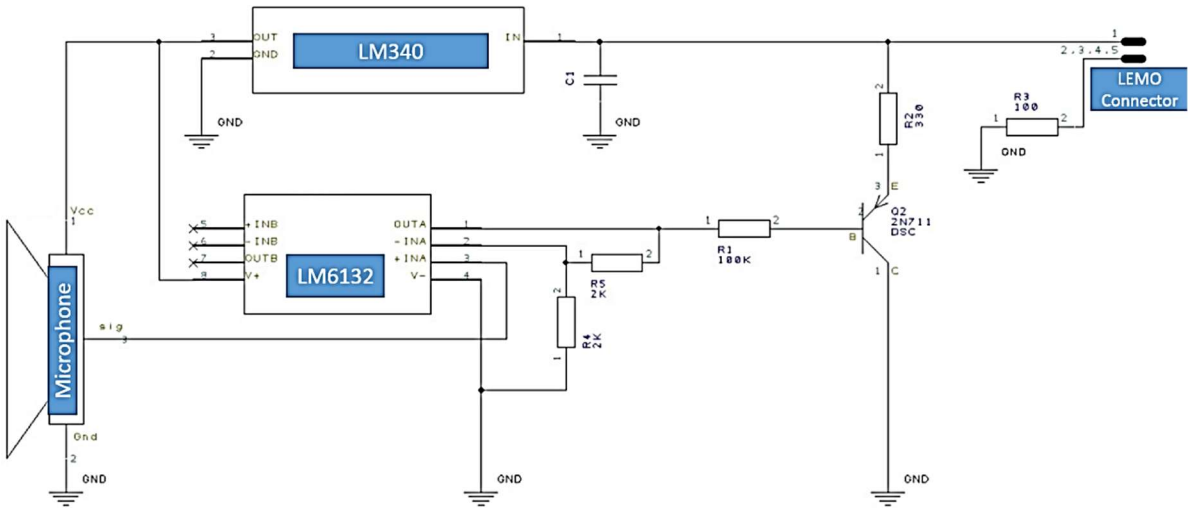

Figure 7. Microphone constant current receiver with temperature compensation.

* Specific vendor and manufacturer names are explicitly mentioned only to accurately describe the test hardware. The use of vendor and manufacturer names does not imply an endorsement by the U.S. Government nor does it imply that the specified equipment is the best available.

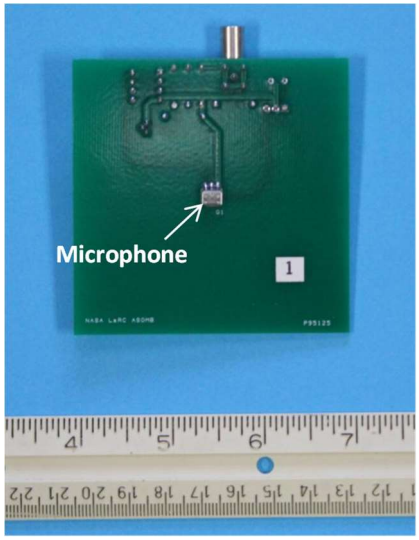

Figure 8. Microphone PCB front side. [Source: NASA]

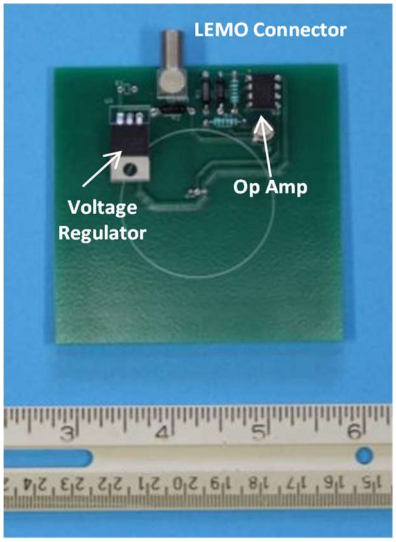

Figure 9. Microphone PCB back side. [Source: NASA]

temperature compensation via a simple voltage regulator (an LM340) and op amp (an LM6132). Figures 8 and 9 show respectively the front and back sides of the microphones, constructed in-house at LaRC on 3-by 3-inch printed circuit boards (PCBs) and using a LEMO® connector to provide power and signal access to the board. A total of 269 microphones of the type shown in Figures 8 and 9 were fabricated (185 for the array plus spares).

Microphone Mounting: Two different types of microphone mounting structures were fabricated for the phased array. The first was a 72-inch diameter central plate populated with the innermost 49 microphones in the array. The plate was manufactured from machined aluminum honeycomb with plastic microphone holders fabricated using an additive manufacturing process. Velcro® strips were used to secure the individual microphone PCBs in the holders. The outer edge of the central plate was treated with contoured foam to minimize acoustic scattering effects. A close-up of the central plate construction highlighting one of the microphone holders can be seen in Figure 10. The completed central plate as deployed in the field can be seen in Figure 11. A protective cover was placed over the plate when the array was not in use.

Figure 10. Close-up of central plate construction. Left – Machined aluminum cutout and holder, Right – Assembled unit [Source: NASA]

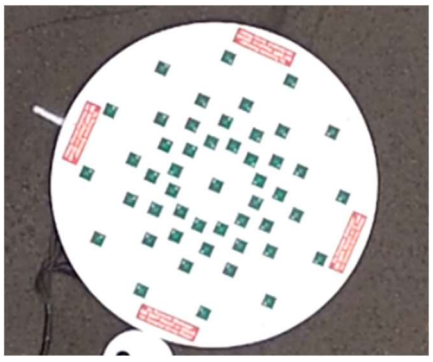

Figure 11. Aerial view of central plate. (From GoPro® camera) [Source: NASA]

The remaining 136 microphones in the array were mounted on individual 12-inch diameter satellite ground plates manufactured from machined white Plexiglass®. Plastic microphone holders identical to those used on the central plate were inserted into the center of each ground plate to secure the microphone PCBs. The edges of the ground plates were contoured to reduce acoustic scattering. Six-inch tall weighted plastic traffic cones were placed over the ground plates when the array was not in operation to protect the sensors from the direct influence of dew and rain. A completed ground plate assembly can be seen in Figure 12.

4.2 Data Acquisition System

Centralized signal conditioning and data acquisition systems were assembled for the array using commercially available hardware. Signal conditioning of all microphone channels was achieved using one of two different architectures (depending on acquisition requirements). The first architecture consisted of an R.C. Electronics, Inc. DTX-9017 programmable signal conditioner assembly populated with DTX-5290 IEPE plug-in cards (4 channels per card) with fully programmable gain and anti-alias filtering available for each channel. The IEPE cards also supplied power to the 4-mA current loops utilized by the microphones. The second architecture consisted of a series of Daqscribe Technologies DSC-2200 programmable signal conditioners also providing full control over gain and filtering of the array channels. The signal conditioner systems were both controlled from a master computer which communicated with individual DTX or Daqscribe channels over a high speed Ethernet connection. The acquisition and digitization system (built by AVEC, Inc.) had a total capacity of 192 channels and was constructed around General Standards Corporation PMC66-16AI64SSA-64-49.152 16-bit synchronous sampling digitizers distributed among three separate PCIe cards. The digitizers were housed in a single high-end computer system with local SSD disk storage. A custom data acquisition module in the AVEC phased array software package[1] was used for command and control of the General Standards digitizers. Acquired microphone time history data were stored on a high capacity NAS device as a series of binary data files. The nominal acquisition window length was 40 seconds for a typical run with all channels sampled at 76.8 kHz and lowpass filtered at 20 kHz. Finally, an IRIG-B UTC timecode signal was acquired on one of the acquisition channels, and served as the mechanism to synchronize the array measurements with recorded flight data on test aircraft. A block diagram of the overall acquisition system is shown in Figure 13.

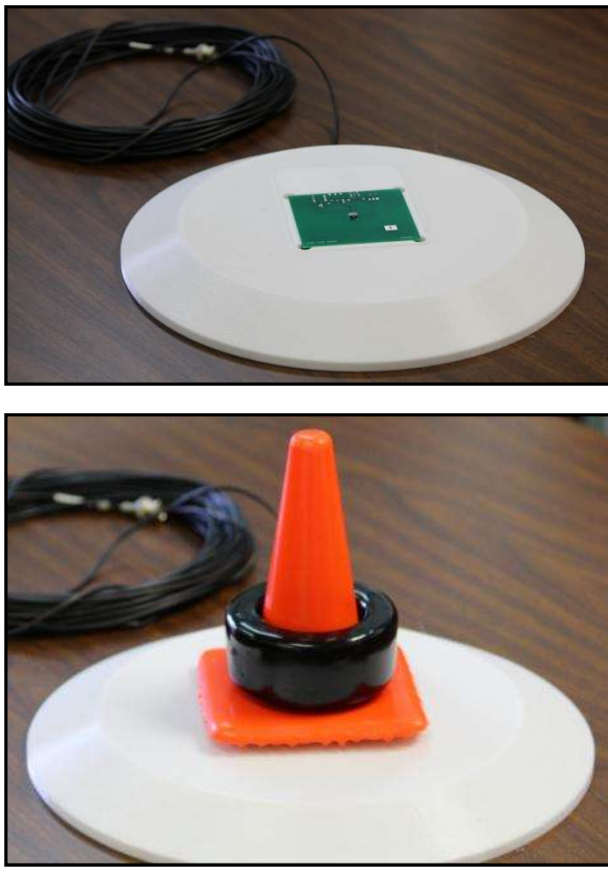

Figure 12. Ground plate assembly.
Top – Plate with PCB inserted
Bottom – Weighted traffic cone protector
[Source: NASA]

[1] http://www.avec-engineering.com/Products.html [cited April 4, 2016].

4.3 Data Analysis System

Aircraft flyover testing requires the application of time-domain processing techniques that can take into account the amplitude and frequency shifts inherent in the time histories recorded by the individual array microphones for the moving noise sources. Consequently, time-delay beamforming was employed to produce contour presentations of noise locations and strengths for flyover datasets. Details of the processing are discussed in this section.

The pressure $p_i(t)$ recorded at microphone i due to a moving monopole source with angular frequency ω, Doppler frequency shift $D_f = f_m/f_r$, and convective amplification $C(t)$ can be represented as [30]

$$p_{i,shi} \quad (t) = A\frac{C(t)}{r_i(t)}e^{j\omega D_f(t)(t-\Delta t_i(t))} \tag{1}$$

where A is the source amplitude, $r_i(t)$ is the time-dependent distance from the source location to microphone i and $\Delta t_i(t)$ is the time-dependent sound propagation time from the measurement location to the microphone. The convective amplification factor $C(t)$ has been investigated by Dowling [31], and the generally accepted formulation for $C(t)$ for a monopole source in motion is given by [32]

$$C(t) = (1 - Mcos\theta_e(t))^{-2} \tag{2}$$

where M is the aircraft Mach number (assumed constant) and $\theta_e(t)$ is the time-dependent propagation path emission angle from the source to the microphone. Convective amplification manifests itself as an increase in the recorded amplitude of moving sound sources upstream of the source location and a decrease in recorded amplitude downstream of the location. The corresponding Doppler frequency shift is given by

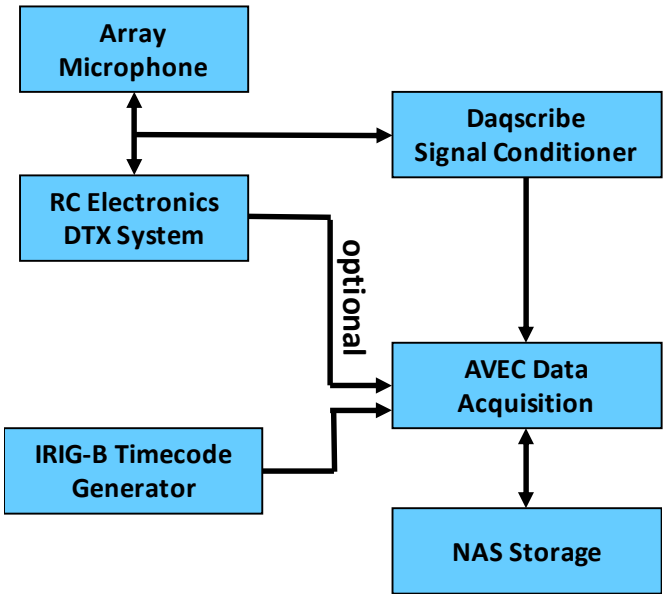

Figure 13. Data acquisition system block diagram.

$$D_f(t) = (1 - Mcos\theta_e(t))^{-1} \tag{3}$$

and implies that the spectral frequencies in the recorded microphone time histories are constantly changing, with true frequencies achieved only when the emission angle is 90 degrees (i.e., when the aircraft is directly over a microphone).

The bias effects manifested in Eqns. (2) and (3) must be removed from the data before beamforming can be performed. This is achieved using aircraft position and orientation data as recorded by a differential GPS tracking system deployed on the aircraft and synchronized with the phased array system. A convective amplification correction is applied to every microphone time history sample. The de-Dopplerization of the time histories requires that the individual time records for all array microphones be shifted and resampled so that blocks of time history information have uniform start times and uniform time steps. There are several detailed explanations available in the literature of how the de-Dopplerization can be performed – the reader is referred to Howell et al. [33] for one example.

For the Langley phased array data analysis system, the data reduction was performed on a multi-core computer using AVEC's flight test software with custom features jointly developed by AVEC and LaRC. One of the features in the GUI included beamforming using a native AVEC code or an imported NASA code (referred to as the BEAMFLY code). Post-processing of the array measurements was conducted using either a conventional delay and sum technique in the time domain or an advanced time domain method described by Dougherty [34]. A regular Cartesian grid was generated that encompassed and moved with the noise sources on the aircraft. The source location and speed were nominally prescribed by differential GPS data describing the position of the aircraft as a function of time. For each potential source location (i.e., grid point), the microphone time histories captured by the array were resampled with time delays and amplitude adjustments corresponding to a monopole moving at locally constant velocity in a homogeneous medium, thereby removing the bias effects in Eqns. (2) and (3). The "delayed" signals were then summed in such a way that the portions of the signals that conform to a monopole at the grid point under observation summed constructively. Array shading (weighting) was employed with individual microphone weights based on the frequency of interest and the microphone location in the array. The weights effectively reduced the array size as the frequency increased, thereby minimizing decorrelation effects among the outer sensors in the array. After applying the shaded delay-and-sum operation, a direct Fourier transform was used to obtain the Fourier coefficients of interest. The coefficients were used in further computations to generate beamform image maps. It is noted that the array processing software contained a feature that allowed automatic exclusion of microphones for which the overall levels were outside a user-defined threshold (in dB or standard deviations from the mean) which in turn improved the beamforming presentations.

Two different corrections for atmospheric attenuation were performed depending on whether atmospheric temperature and humidity profiles were available. When weather profiles were available, a layered correction approach was employed similar to that described by True et al. [35]. This correction stratified the atmosphere into layers of user-defined heights h extending from the ground to the aircraft flyover altitude (see Figure 14). The local atmospheric attenuation was computed for each layer based on the average temperature and humidity within the layer as measured by a weather profiling system (e.g., a radiosonde on a balloon). Within a layer, the distance along the line of sight connecting the location of the aircraft (from the GPS tracking) and an array microphone was used to compute the total dB loss of sound within the layer. These separate dB losses were then summed to obtain the total loss from the aircraft location to the microphone. The total correction to add to an individual microphone's output as a function of source frequency was given by

$$dB_{total,mic}(f) = \sum_{i=1}^{n} dB_{i,mic}(f, T_i, H_i, d_i) \tag{4}$$

where f is the source frequency and $dB_{i,mic}$ is the computed dB loss across the ith atmospheric layer (with average temperature T_i and humidity H_i over a distance $d_i = h/\cos(\xi)$) within a total of n layers. The atmospheric attenuation for each layer was determined according to ANSI standard S1.26-1978 [36].

For those cases where a weather profile was not available, it was assumed that the atmosphere was uniform in temperature and humidity from the aircraft altitude AGL to a microphone. Thus, only a bulk atmospheric attenuation and associated $dB_{total,mic}$ loss correction were computed and applied to the array microphones.

Further processing of the data could be performed using deconvolution methods that take into account the actual array response to a moving monopole at each of the source locations. The deconvolution methods available in the AVEC flight test software included the DAMAS, CLEAN, and CLEAN-SC algorithms [15, 37]. Source integrations could be performed over selected regions of interest in the beamform image maps after the deconvolution of the data has been completed.

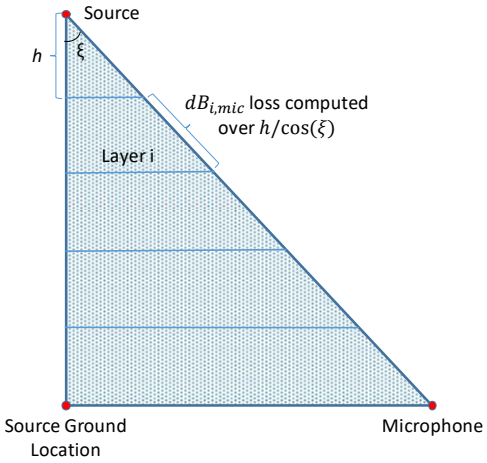

Figure 14. Layered atmospheric attenuation correction geometry.

4.4 Supporting Instrumentation

The complete ensemble of data acquisition and quick-look data analysis hardware for the array system was housed in a command trailer (Figure 15) that could be positioned up to 200 feet from the edge of the array (assuming a 200-foot diameter array connected to the trailer using the 400-foot, LEMO®-terminated cables described previously). The trailer was equipped with a commercial 30-foot weather station that utilized a sonic anemometer for wind speed and direction, an aspirated temperature / humidity sensor, and a barometric pressure gauge. The weather station performed time-stamped sampling of the local conditions on 5-second intervals, with 1-minute averages also computed. The resultant 5-second and 1-minute weather files were stored on the NAS device along with the microphone time histories. The command trailer was also equipped with three available surveillance video cameras connected to a digital video recorder for monitoring and recording of all aircraft passes over the array. The cameras were attached to pan/tilt gimbal mounts to allow proper orientation of the individual fields of view.

Figure 15. Command trailer for array. [Source: NASA]

5.0 Characterization of Microphone Performance

Measurements of absolute microphone sensitivity, frequency response, total harmonic distortion, and noise floor were performed via a bench top calibration of all sensors both before and after each array deployment. The calibrations were conducted using a Bruel and Kjaer 4226 multifunction calibrator as a precision sound source and a National Instruments USB 9215 digitizer to record both the reference signal from the calibrator and the output of the microphone (see photo in Figure 16 and a block diagram of the setup in Figure 17). The sensitivity and total harmonic distortion were measured using a 250-Hz, 94-dB SPL tone, corresponding to a pressure excitation of one Pascal at the microphone. The frequency response was measured by applying a broadband white noise signal to the external input port of the 4226 calibrator. The noise floor of the microphone was measured by shutting down the calibrator while leaving the calibrator head on the microphone to simulate a quiescent condition. In all cases, a sampling rate of 100 kHz with an acquisition time of 5 seconds was employed for the measurements.

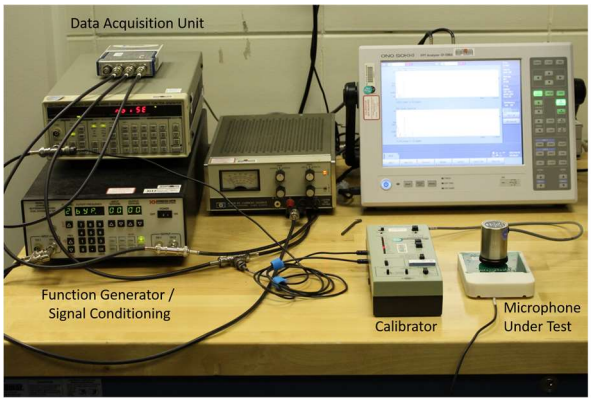

Figure 16. Benchtop calibration hardware. [Source: NASA]

5.1 Laboratory Calibration of Microphones

Sensitivity: Representative histograms of microphone sensitivities measured immediately after the fabrication of the sensors as well as after multiple deployments of the array are shown in Figure 18. Note that the total number of microphones calibrated for each deployment varied slightly as additional sensors were fabricated or as sensors failed during deployment. The distribution of the sensitivities is approximately Gaussian in shape in all cases, with the overall mean sensitivity for the sensors shown in each figure panel. It is further noted that the histogram data shown in Figure 18 were used as selection criteria for choosing the best "matched" microphones for incorporation into the array. Sensors with sensitivities at the outer edges of the distribution (typically exceeding two standard deviations from the mean) were identified as spares.

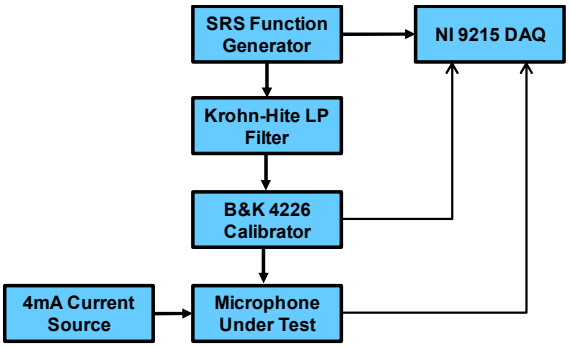

Figure 17. Block diagram of calibration setup.

In general, the stability of the microphone sensitivities was excellent over the four-year period represented in Figure 18 (fabrication of the initial batch of microphones was completed in 2014 with the last deployment of the array conducted in 2018). While some variation in the shape of the histograms is observed in the figure, the mean value of the sensitivity for the entire ensemble of microphones remained remarkably consistent, implying that very little sensitivity drift was observed for the sensors.

Total Harmonic Distortion (THD): Representative histograms of THD for the entire ensemble of fabricated microphones are shown in Figure 19. The harmonic distortion was computed as a percentage for each sensor using [38]

$$THD = \sqrt{\frac{A_2^2+A_3^2+\cdots+A_7^2}{A_1^2+A_2^2+A_3^2+\cdots+A_7^2}} x\ 100 \quad (5)$$

where A_1 is the amplitude of the fundamental 250-Hz, 94-dB sound pressure level signal applied to the microphone and A_2, A_3, …, A_7 are the amplitudes of the first six harmonics obtained using a modified periodogram method.

Some variability is shown in the individual histograms in Figure 19. In particular, there were some undocumented changes made to the procedure for collecting the THD data after the 2017 Edwards AFB deployment that resulted in a tighter distribution of THD values for the microphones. It is conjectured that the histograms shown in Figures 19(e) and 19(f) are more representative of the true distributions for the ensemble of microphones, with mean THD values approaching 1%.

Noise Floor: Representative histograms of the unweighted noise floor for the entire ensemble of fabricated microphones are shown in Figure 20. Although the histograms shown in the figure approximate Gaussian distributions, approximately 5 percent of the sensors appear at the higher outer edge of the distributions, which are indicative of elevated noise floors. It is noted that the mean values of the histogram distributions increased slightly as the microphones were used in multiple deployments. It is uncertain whether this increase occurred due to aging of the microphone cartridge itself or whether the increase in noise floor was due to aging in the 4mA constant current circuitry on the back side of the microphone circuit boards.

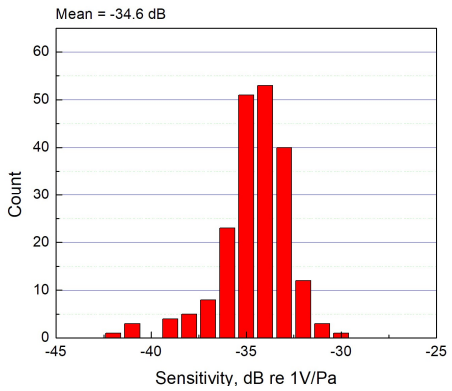

(a) Post-fabrication calibration

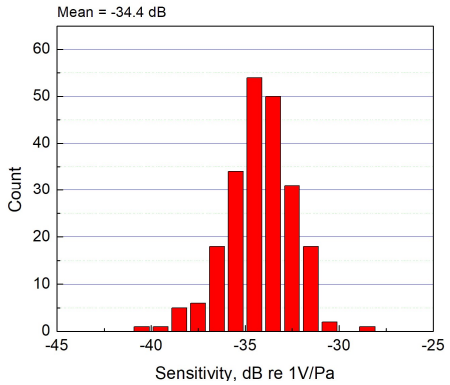

(b) Pre-AP Hill calibration

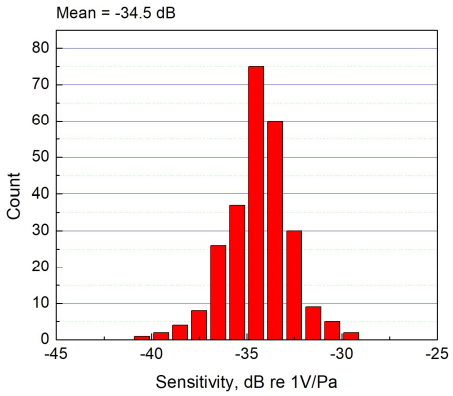

(c) Post-AP Hill calibration

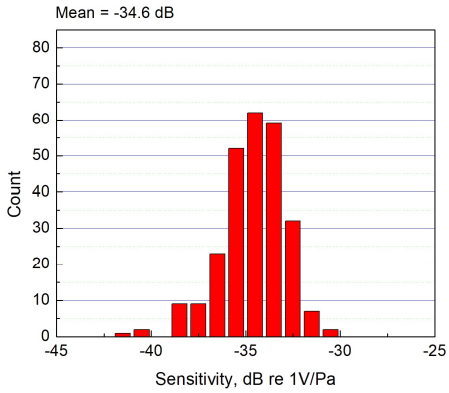

(d) Post-2016 Edwards AFB calibration

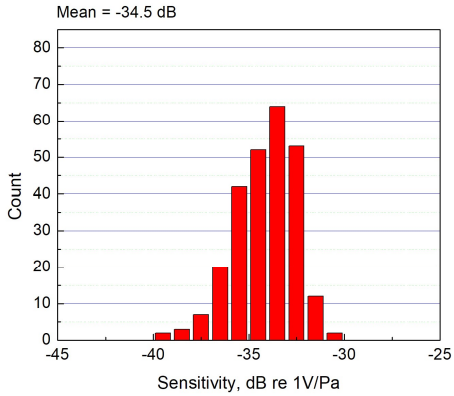

(e) Post-2017 Edwards AFB calibration

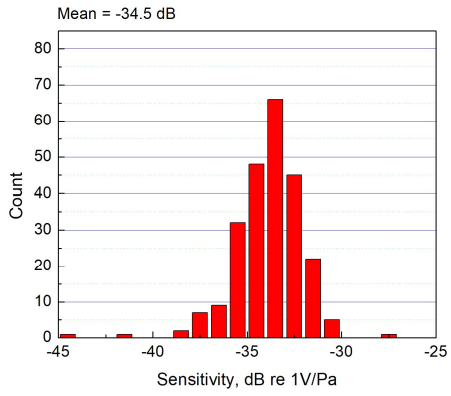

(f) Post-2018 Edwards AFB calibration

Figure 18. Representative distributions of microphone sensitivities measured after initial fabrication and after deployments.

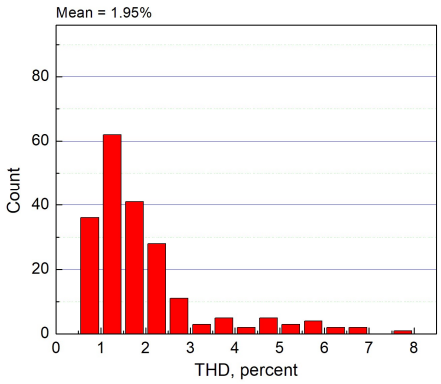

(a) Post-fabrication calibration

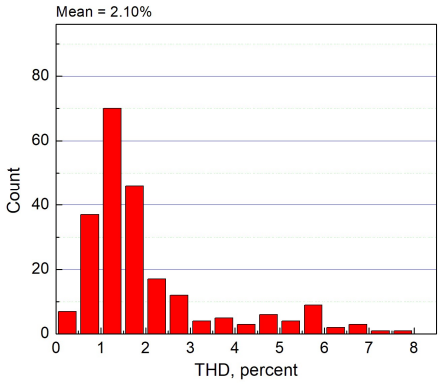

(b) Pre-AP Hill calibration

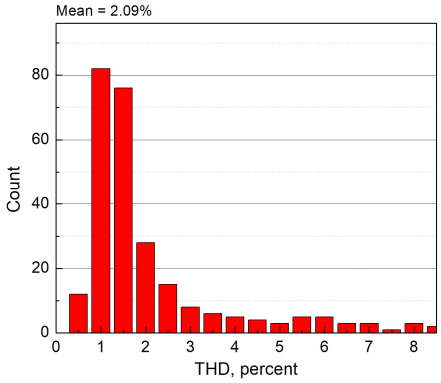

(c) Post-AP Hill calibration

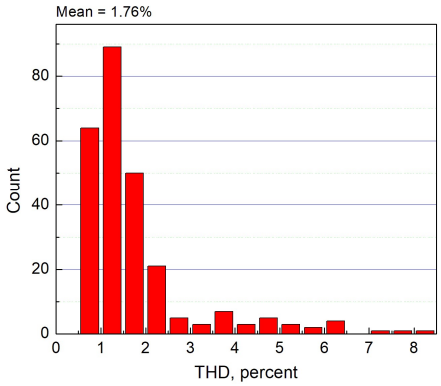

(d) Post-2016 Edwards AFB calibration

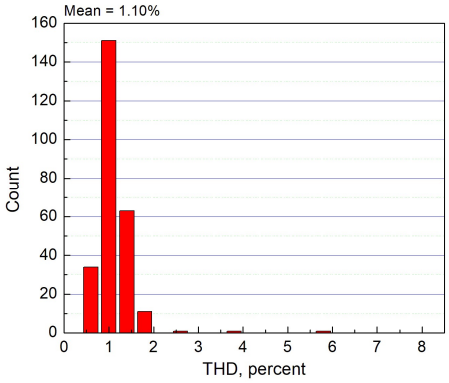

(e) Post-2017 Edwards AFB calibration

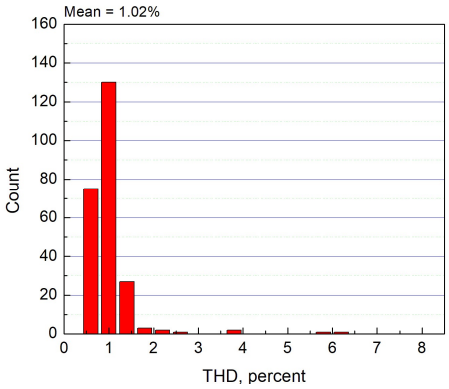

(f) Post-2018 Edwards AFB calibration

Figure 19. Representative distributions of total harmonic distortion measured after initial fabrication and after deployments.

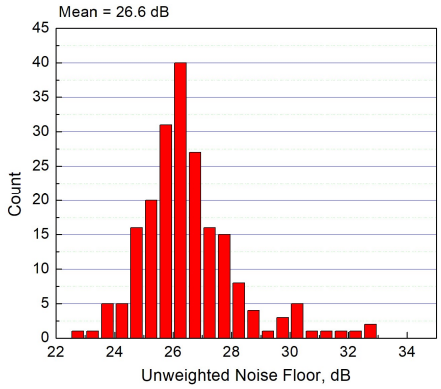

(a) Post-fabrication calibration

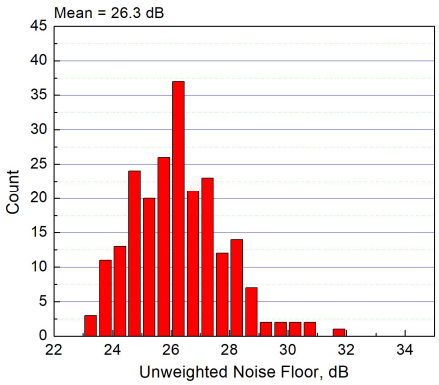

(b) Pre-AP Hill calibration

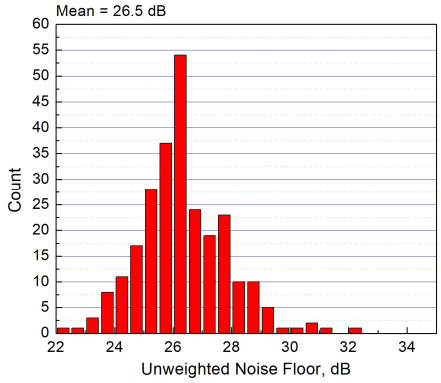

(c) Post-AP Hill calibration

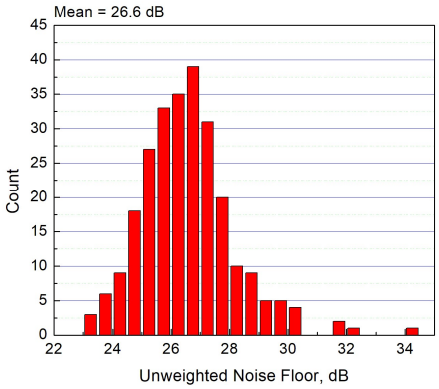

(d) Post-2016 Edwards AFB calibration

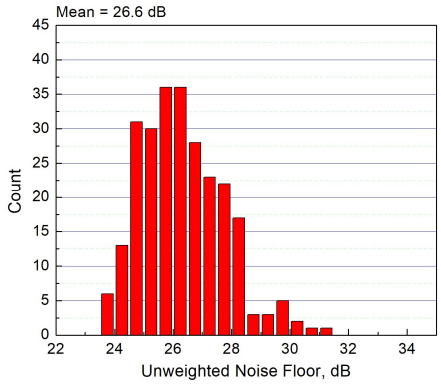

(e) Post-2017 Edwards AFB calibration

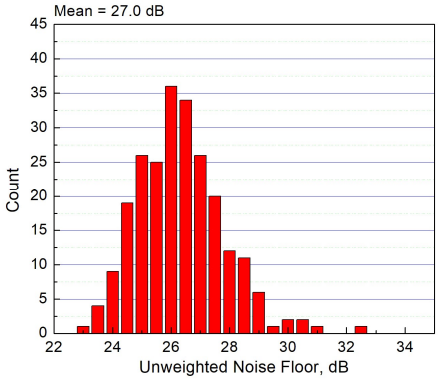

(f) Post-2018 Edwards AFB calibration

Figure 20. Representative distributions of unweighted noise floors measured after initial fabrication and after deployments.

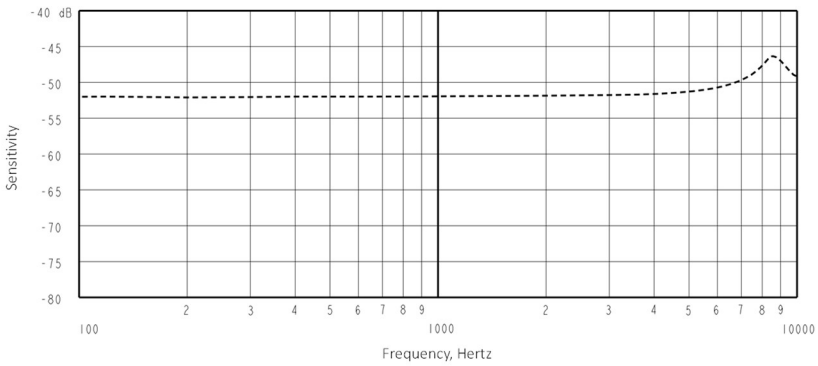

Figure 21. Typical WP-23849 frequency response.

Frequency Response: A typical frequency response for the Knowles WP-23849 microphone is shown in Figure 21. The microphone exhibited a flat frequency response from 100 Hz to 6 kHz with the first diaphragm resonance peak occurring at 8.5 kHz. This frequency response was deemed acceptable since the highest frequency of interest was approximately 7 kHz for the test campaigns using these microphones.

5.2 Characterization of Microphone Directivity

The microphone cartridge shown in Figure 8 utilized three pinholes for allowing the sound waves to reach the diaphragm, thus it was necessary to measure the directivity of the microphones to determine if any amplitude or phase corrections would be necessary during flyover testing using the array. The directivity measurements were conducted in the Langley Structural Acoustic Loads Transmission (SALT) anechoic facility. Acoustic speaker holders and microphone casings were 3D-printed from CAD models for installation in the facility (Figures 22 and 23) [39]. The microphone holder was mounted on a Zaber rotation stage controlled from a LabVIEW® program (Figure 24) to rotate the test microphones in 4-degree steps over a -90 to +90 degree angular range. Ten different microphones were tested where five seconds of data

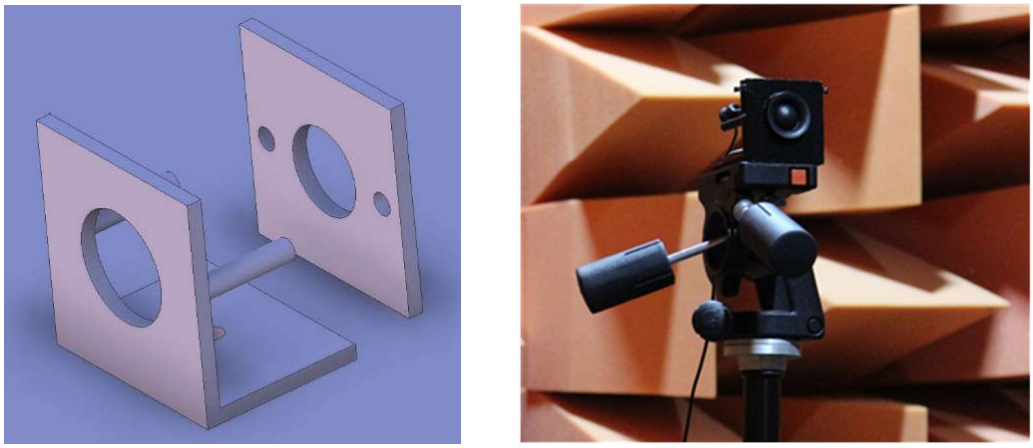

Figure 22. Acoustic source mount for directivity measurements in the SALT.

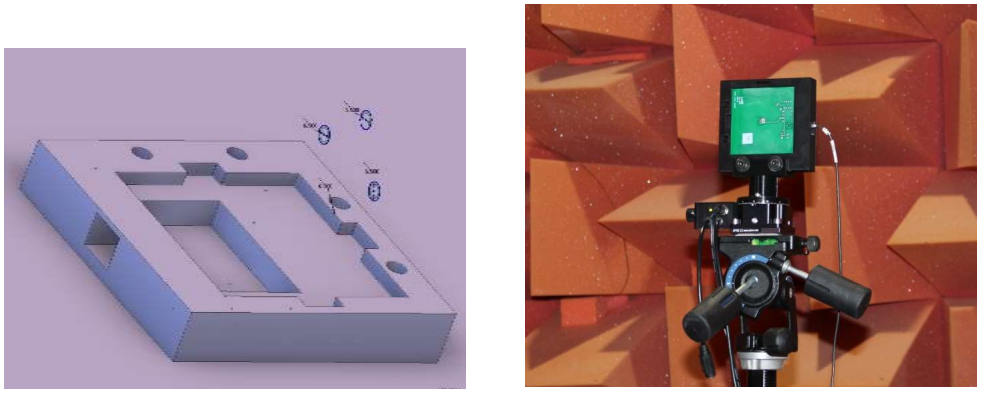

Figure 23. Microphone casing for directivity measurements.

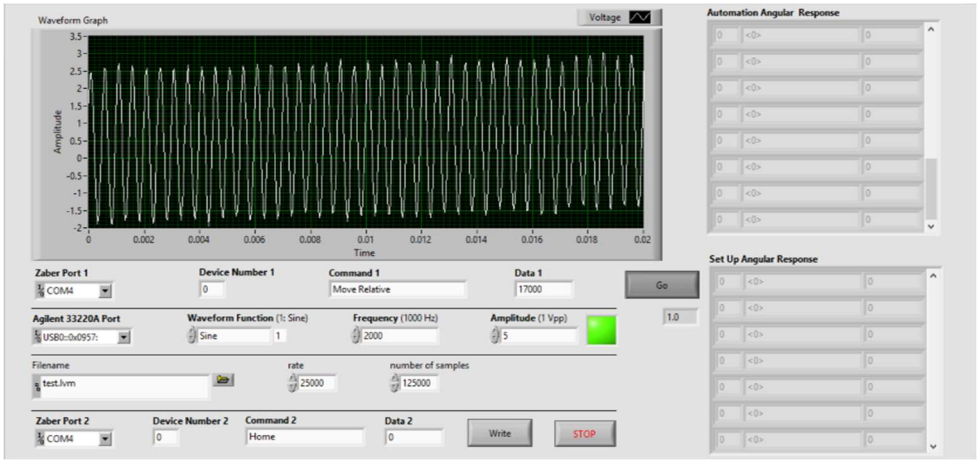

Figure 24. Developed LabVIEW® code for directivity measurements.

were acquired at a 25-kHz sampling rate for each microphone angle setting, with the microphones tested in both the azimuthal and polar planes (by physically rotating the microphone circuit board in the holder shown in Figure 23).

Figure 25 shows representative polar plane directivity profiles for a single microphone over a range of source frequencies spanning 2 to 8 kHz. For frequencies under 5 kHz, the directivity exhibited the shape of a partial bi-directional or figure-of-eight profile. The coverage pickup spanned ±60 degrees with a maximum response perpendicular to the microphone. A non-standard directivity pattern was exhibited at 6 kHz where two strong sidelobes in the profile were evident, angled at approximately ±45 degrees. The lack of a strong main lobe at this frequency could be problematic for certain aircraft emission angles. As the frequency extends to 8 kHz, a main lobe reappeared in the profile with two strong sidelobes again appearing at approximately ±50 degrees. It is speculated that the unusual profiles exhibited by the microphone at higher frequencies could be due to two influences: (1) the profiles could be directly related to the geometry of the three pinholes on the front surface of the sensor (see Figure 8), and (2) the relatively small size of the mounting plate might have caused undesired edge effects. Although this was not tested, two of the pinholes could be sealed in an attempt to improve the high frequency profiles, and a bigger mounting plate similar to the one shown in Figure 12 could be used to investigate edge effects. Nevertheless, the overall directivity performance of the microphone was considered acceptable.

Figure 26 shows representative azimuthal plane directivity profiles for a single microphone for the same range of frequencies spanning 2 to 8 kHz. The observed profiles are virtually identical to those shown for the polar plane, implying that the microphone is relatively insensitive to orientation in the plane of the array. This is an important finding since it can be difficult to control microphone orientation when deploying an array.

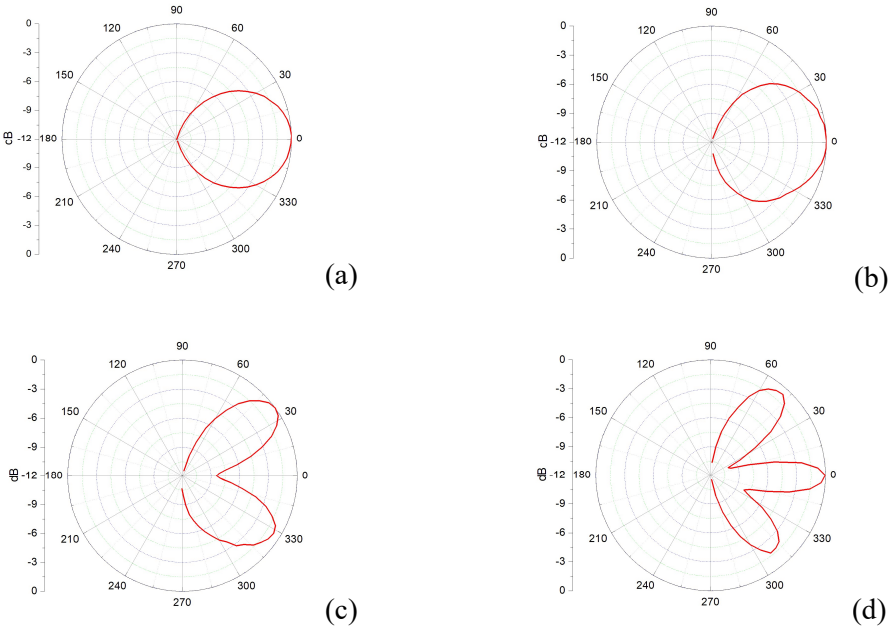

Figure 25. Microphone polar directivity profiles.
Source frequency: (a) 2 kHz, (b) 4 kHz, (c) 6 kHz, (d) 8 kHz

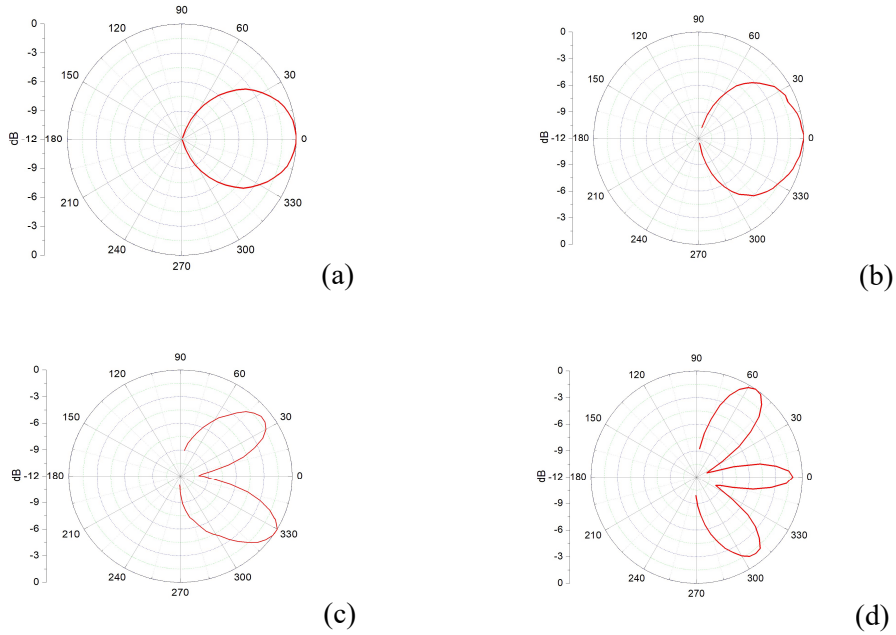

Figure 26. Microphone azimuthal directivity profiles.
Source frequency: (a) 2 kHz, (b) 4 kHz, (c) 6 kHz, (d) 8 kHz

6.0 Array Mockup in Langley Acoustic Development Lab (ADL) - 2014

A detailed mock-up of the instrumentation suite (phased array, weather station, and data acquisition and processing) was performed in the LaRC Acoustic Development Laboratory (ADL) prior to the first outdoor deployment of the array to: (1) identify any anomalies in the operation of the system that needed correcting, and (2) vet the microphone and overall system performance. Due to space constraints, a simplified and much smaller array pattern than would normally be used was deployed in the test chamber, as shown in Figure 27. Although 185 microphones were available for testing, the space constraint dictated the use of only 163 microphones in the tested array. Appendix A lists the design coordinates for the array, and Figure 28 depicts the final setup of the array hardware in the facility.

A 1-inch diameter tube connected to a voice-coil speaker driver was suspended approximately 13.5 feet over the center of the array and used as a pseudo monopole point source, exciting the array sensors with tones and white noise. Figure 29 depicts the typical response of the ADL mock-up array when excited with 1-, 2-, and 4-kHz pure tones. These are compared with theoretical point spread functions computed from the array pattern for like frequencies. In general, good agreement is observed between the theoretical and experimental point source responses of the array. There are higher sidelobe levels observed for the experimental responses versus theory, especially for the 1- and 4-kHz tones. However, it is noted the ADL is only a partially anechoic environment with the sidewalls treated for acoustic reflections and not the ceiling or floor. This can result in an overall degradation of array sidelobe performance. Also, while the central mounting plate was accurately positioned in the test chamber, the locations of the individual ground plates were only accurate to ±1 inch, contributing to higher measured sidelobe levels compared with theory.

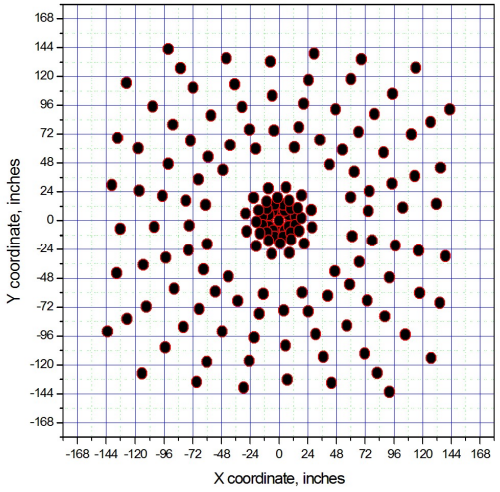

Figure 27. Array pattern deployed in ADL.

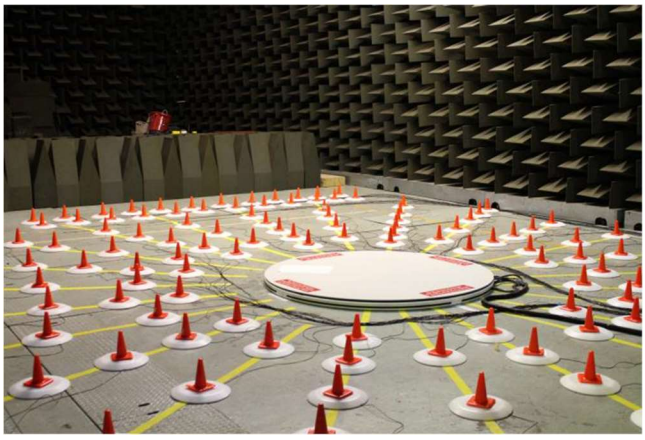

Figure 28. Completed ADL array mock-up.

While in general the array operation was nominal during the ADL mock-up, reliability issues regarding the operation of the data acquisition system were noted. These issues ultimately resulted in the replacement of the data acquisition system with the AVEC system noted in Section 4.2. Also, management of the 185 microphone cables was a problem during the mock-up, so improved cable management methodologies were implemented. It was also discovered during the ADL mockup that additional moisture protection was needed for the circuitry on the front and back of the microphone printed circuit boards (refer to Figures 8 and 9). Hence, to improve the hardening of the microphones, the populated PCBs were conformal coated with an acrylic sealant to render the circuitry on the front and back of the boards waterproof. Figure 30 shows one of the microphones with the coating applied. The coating was effective at improving the robustness of the microphones during deployment.

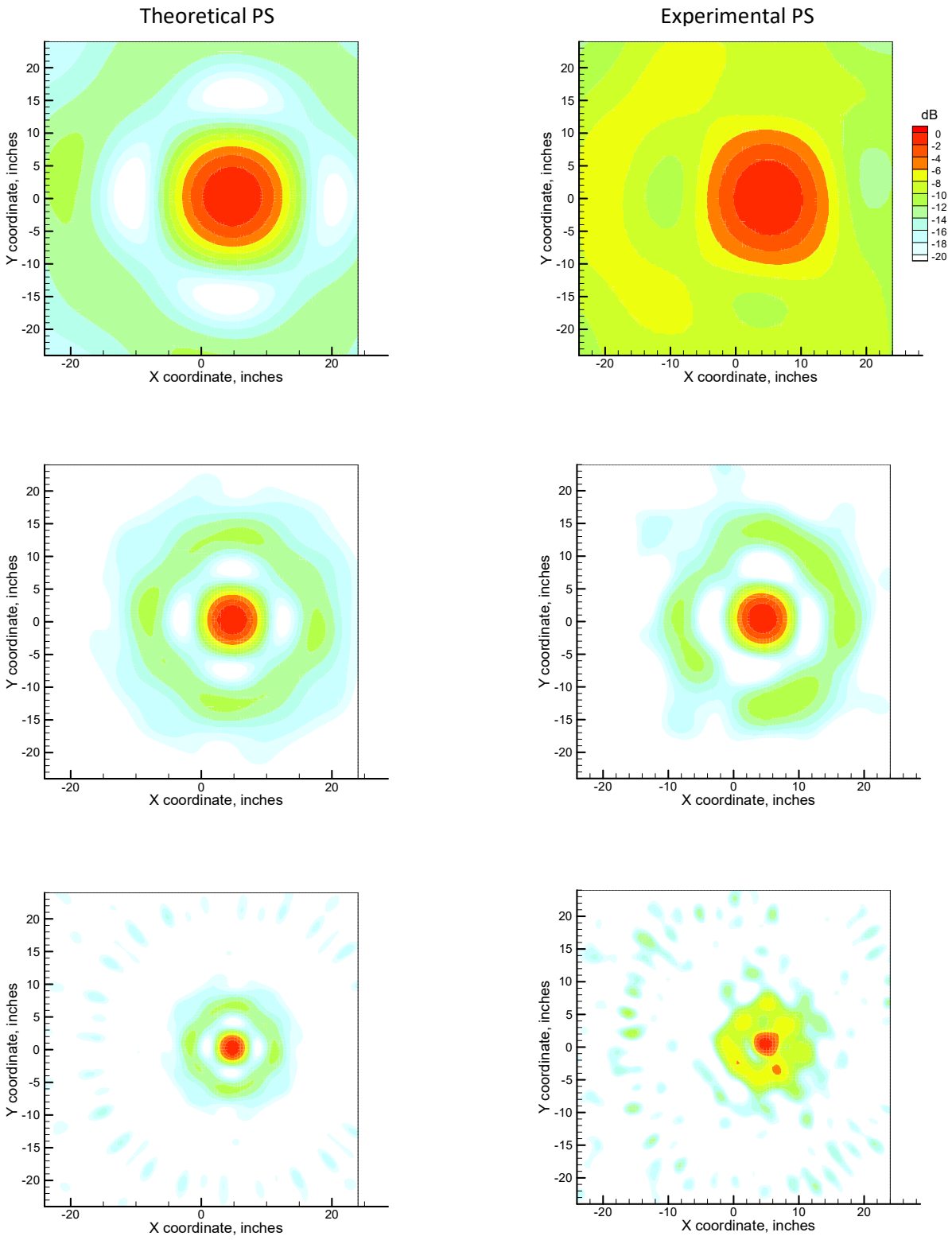

Figure 29. Comparison of narrowband ($\Delta f = 75$ Hz) beamform maps for theoretical and experimental point sources for array mockup in ADL. Top – 1-kHz Tone, Middle – 2-kHz Tone, Bottom – 4-kHz Tone

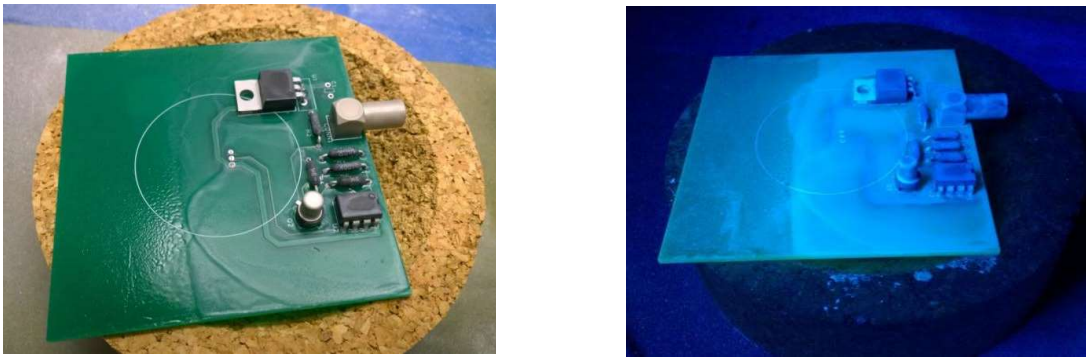

Figure 30. Conformal coating of microphone PCB to protect electronics. Coating was concentrated on PCB end containing components. [Source: NASA]
Left – visible light, Right – Ultraviolet light

7.0 Shakedown Testing of Array at Fort A.P. Hill – 2015

Shakedown testing of the new array design occurred at Finnegan Airfield at Fort A.P. Hill in late August 2015, where the array was utilized to measure vehicle noise for a number of sUAS (small Unmanned Aerial System) aircraft.

Test Site: Located in Eastern Virginia, Finnegan Airfield is a paved sUAS runway approximately 1200 feet long and 75 feet wide with a small slope from the east to west end. It is used for U.S. Army unmanned aircraft system training at Fort A.P. Hill. The runway is operated within restricted airspace and is flanked by tree lines to the north 180 feet away and to the south 200 feet away. A small hangar is located 110 feet to the north of the runway for sUAS aircraft staging and maintenance, and an automated ground weather station (accessible via the internet) is available at the west end of the runway.

Array Pattern and Deployment Details: The array deployed at Finnegan consisted of 185 microphones arranged in an irregular starburst pattern 79 feet wide and 93.7 feet long (Figure 31 - see Appendix B for

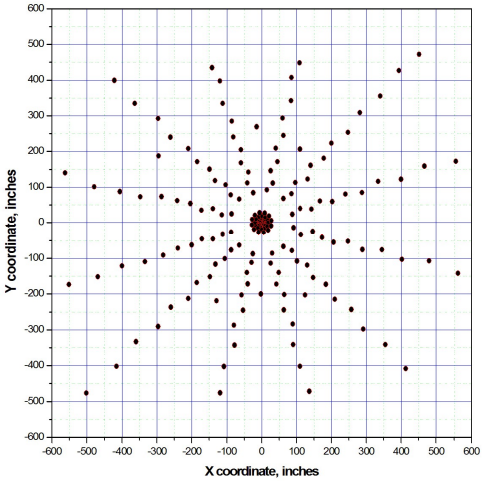

Figure 31. Array pattern at Finnegan.

Figure 32. Aerial view of array deployment at Finnegan. [Source: NASA]

the design microphone coordinates). The array was positioned at the east end of the runway with the edge of the array aperture 35 feet from the runway threshold. An aerial photo of the deployment is shown in Figure 32. The central 49 microphones of the array were housed on a central mounting plate with the remaining 136 microphones housed on individual ground plates as described in Section 4.1. The array was designed for an operational frequency range of approximately 1-10 kHz. Three additional Bruel and Kjaer freefield microphones were deployed as reference microphones, with one located near the array central mounting plate, one located approximately 70 feet directly up-range of the array along the runway centerline, and one located approximately 70 feet laterally from the edge of the array on the south side of the runway. The command trailer for the array was positioned in the grass on the north side of the runway approximately 75 feet from the edge of the array aperture.

Testing: Vetting of the phased array system was achieved by acquiring data for a number of Langley sUAS aircraft that passed over the center of the array at a nominal 100-foot altitude using an engine idle descent trajectory. The tested vehicles (managed by the Langley UAS Operations Office) included two J-FLiC (Jet-powered Flying Controls testbed) KingCat aircraft (N508NU, N509NU) and a Langley Research Services Directorate (RSD) 40-percent scale Carbon Cub propeller-driven aircraft (N383NA). The J-FliC is shown passing over the array microphones in Figure 33. Over 200 individual sets of acoustic data were acquired during the deployment at Finnegan, spanning a total of 7 testing days. The array's operation was nominal during this time, with only 8 microphones out of 185 exhibiting problems requiring replacement with backup units, despite the sensors being subjected to extremes of temperature and humidity during the deployment. Lessons learned during the Fort A.P. Hill tests were used to improve the performance of the array prior to operational deployments. These included changes to the data acquisition system and development of various methods for array health monitoring as discussed in Section 9.0.

Figure 33. J-FliC flight over array.

8.0 Operational Array Deployments – 2016, 2017, 2018

Following the successful shakedown tests that were completed at Fort A.P. Hill, three separate deployments of the array were conducted at Edwards AFB in California during a two-year period from 2016 through 2018. The array was utilized to obtain full-scale evaluation data for promising airframe noise reduction technologies in a relevant environment, using two NASA Gulfstream G-III aircraft outfitted with landing gear and flap noise reduction devices (Figures 34 and 35) [40 – 42]. The flight tests were referred to as the Acoustics Research Measurements (ARM) campaigns. Table 1 lists some details for these campaigns.

Table 1. ARM Campaign Details.

Campaign	Location	Aircraft	Goals
ARM-I (2016)	Edwards AFB Runway 18L	G-III, NASA 804 and NASA 808*	Evaluation of Adaptive Compliant Trailing Edge (ACTE) flap noise reduction
ARM-II (2017)	Edwards AFB Runway 18L	G-III, NASA 804 and NASA 808	Evaluation of main landing gear and gear cavity noise reduction concepts along with ACTE flaps
ARM-III (2018)	Edwards AFB Runway 24 (inactive)	G-III, NASA 804 and NASA 808	Evaluation of main landing gear and gear cavity noise reduction concepts with conventional flaps

* Tail numbers for aircraft.

Figure 34. NASA 804 aircraft. [Source: NASA]

Figure 35. NASA 808 aircraft. [Source: NASA]

Test Site: The array was deployed at the north end of Edwards runway 18L for the 2016 and 2017 deployments. This runway is situated on a dry lakebed and provided an excellent flat surface for deployment of the microphones. Testing for the 2018 deployment occurred in the spring when more frequent rain events occur at Edwards AFB. Thus, the array was deployed on the overrun section of inactive runway 24 for this test campaign. Aerial views of the array deployed on the two runways are shown in Figures 36 and 37. The small black patterned targets shown embedded within the array in Figure 37 were used for optical geolocation of the Mark II acoustic calibration vehicle described in Section 9.0 [43].

Figure 36. ARM-I and ARM-II array deployments on Edwards AFB runway 18L. [Source: NASA]

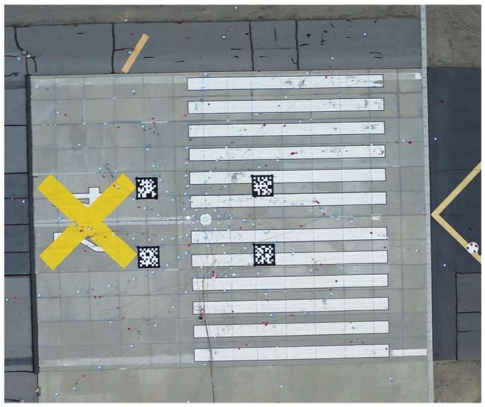

Figure 37. ARM-III array deployment on Edwards AFB inactive runway 24. [Source: NASA]

Array Pattern and Deployment: The array pattern for all three test campaigns consisted of 185 microphones arranged in an irregular spiral pattern with a 250-foot diameter (Figure 38 – see Appendix C for a list of microphone design coordinates for the array). As was conducted in the shakedown tests at Fort A.P. Hill, the central 49 microphones of the array were housed on a central mounting plate with the remaining 136 microphones housed on individual ground plates. The array was designed for an operational frequency range of approximately 300 Hz – 8 kHz. Three additional Bruel and Kjaer freefield microphones were deployed around the array for use in Effective Perceived Noise Level (EPNL) measurements. The command and control trailer was positioned approximately 100 feet from the edge of the array aperture. For the ARM-III deployment, all the microphone cables were wrapped in a mixture of metal sleeving, Kevlar fabric, and plastic tape to protect them from wildlife present in the desert area adjacent to runway 24.

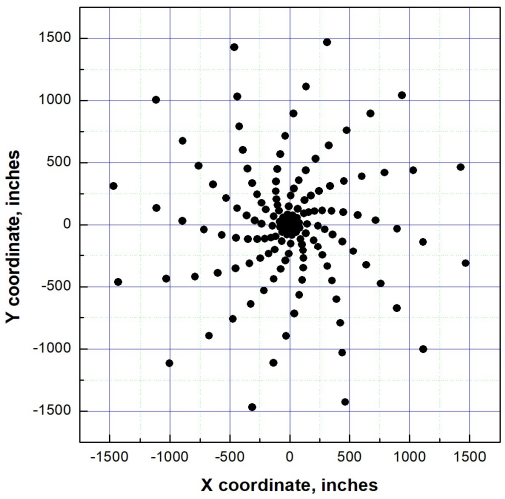

Figure 38. Edwards array pattern.

Testing: The array flyovers were executed in a racetrack pattern (Figure 39) with the aircraft engines operating at "ground-idle" to minimize contamination of the acoustic measurements by propulsion noise. To ensure that the gathered data were statistically meaningful, multiple passes during each flight and repeat flights on different days were executed for most of the aircraft configurations in Table 1. To determine velocity scaling, acoustic measurements were obtained at nominal speeds of 140, 150, and 165 kts with the middle value representing the speed at which the majority of the measurements were taken. Since the ARM-I, II, and III campaigns spanned two years, a large ensemble of pass-to-pass, day-to-day, and year-to-year variations in the measured noise signatures were able to be acquired and assessed.

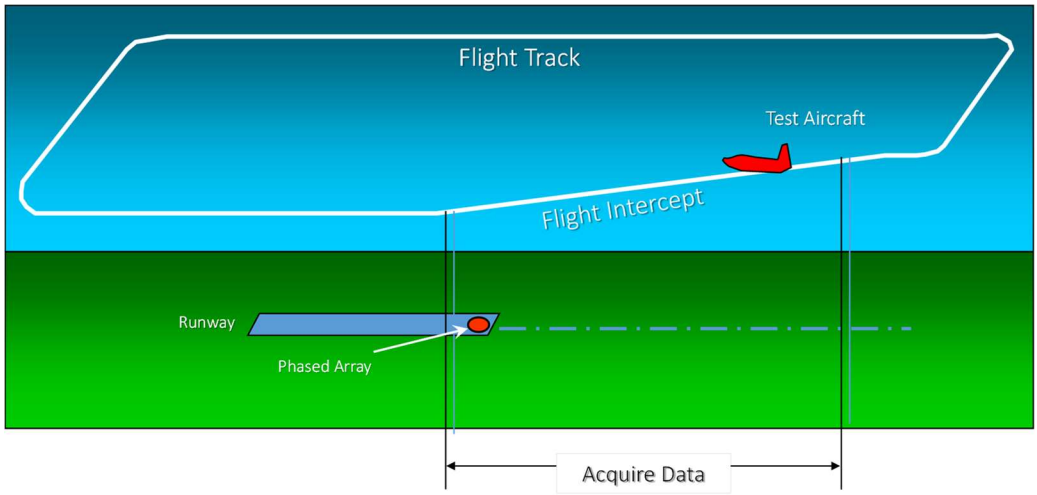

Figure 39. Racetrack pattern for ARM test campaign array data acquisition.

Sample beamform data (using the CLEAN deconvolution algorithm) acquired by the array for passes of the baseline NASA 804 aircraft with a flap deflection of 39 degrees and with the landing gear deployed can be seen in Figure 40. Three 1/12-octave band frequencies are shown representing low-, medium-, and high-frequency noise content. The noise maps have been normalized for each panel in the figure by subtraction of the maximum SPL for each frequency, thus allowing a direct comparison for the location, strength, and shape of the noise sources. The maps in the left and middle columns correspond to two consecutive aircraft passes (no. 4 and 5) executed during March 20, 2018 and those on the right column belong to pass no. 9 executed on March 30, 2018. The data shown illustrates that the array was fully capable of identifying predominant airframe noise sources and distributions on the aircraft during flight, validating that the performance of the array was adequate to meet the measurement goals of the ARM test campaigns. The reader is referred to [41 – 42] to view additional test data acquired by the array during ARM testing.

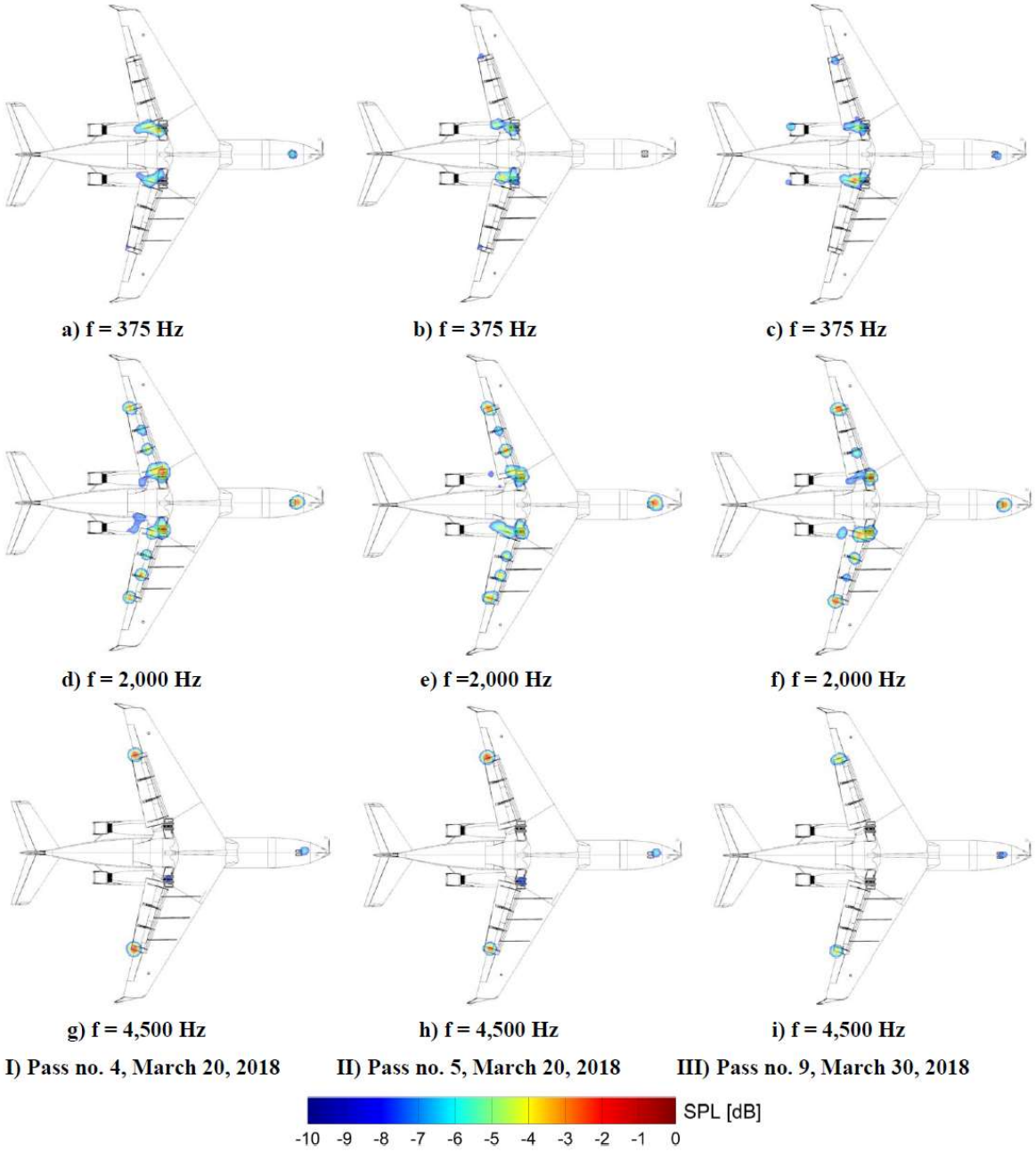

Figure 40. Representative baseline 1/12-octave CLEAN beamform data acquired by the ARM-III array on the NASA 804 aircraft. From Reference 42.

9.0 Development of In-Situ Array Health Monitoring

A critical aspect of daily array operation involved executing health monitoring procedures and measurements whereby daily in-situ array sensor response and channel performance data could be obtained for the duration of the deployment. This was a non-trivial task, given the constraints imposed by the ambient environment (i.e., weather conditions, background noise) as well as the large size of the array aperture. In general, it was not practical to perform a daily calibration of each individual microphone in the array. Therefore, global methods for tracking the health of all of the array elements were employed. There were two particular methods developed that are described here: (1) a unique in-situ calibration method using a hovering aerial sound source, and (2) a multiple ground-source calibration method.

9.1 Aerial Sound Source

A unique in-situ calibration method for the array sensors was attempted for the first time during the Fort A.P. Hill and Edwards AFB deployments using a hovering aerial sound source. In principle, comparison of recorded microphone output levels during flights of the sound source allows the relative response drift of the sensors to be tracked on a daily basis, as long as the effects of speaker directivity, sound propagation (including meteorological conditions) and vehicle station keeping are taken into account. There are many challenges to overcome with this type of array health monitoring: (1) minimizing the position error of the vehicle relative to the array, (2) accurately determining the attitude of the vehicle (roll and pitch) since these can affect the directivity of the aerial sound source, (3) isolating propeller noise from the measurements, (4) estimating contributions from wind noise, and (5) characterizing the background noise environment. A comprehensive effort was undertaken to understand and mitigate these challenges.

Two different sUAS vehicles were chosen to host the aerial sound source payload, denoted here as the Mark I and Mark II Acoustic Calibration Vehicles (ACVs). The salient features of each of these vehicles are summarized in Table 2.

Table 2. Acoustic Calibration Vehicle Specifications.

	Mark I ACV	Mark II ACV
sUAS Type	Multi-Rotor, 6 Brushless Motors	Multi-Rotor, 8 Brushless Motors
Manufacturer	Prioria Robotics	DJI
Diagonal Length	31 inches	41.1 inches
Maximum Weight	16.6 lbs	24.3 lbs
Landing Rails	Fixed	Retractable
Speed	0 – 23 knots	0 – 42.5 knots
Endurance	25 minutes	15 minutes
Command and Control	Remote Control Ground Station	Remote Control Ground Station
Sound Source Payload	Anchor MiniVox Lite PA Speaker	Anchor MiniVox Lite PA Speaker

Figure 41. Mark I ACV at Fort A.P. Hill. [Source: NASA]

Figure 42. Mark II ACV at Edwards AFB. [Source: NASA]

The Mark I ACV consisted of a Prioria Robotics Hex Flyer with a suspended battery-powered Anchor® MiniVox Lite public address speaker and MP3 player as the payload. The vehicle is shown in flight in Figure 41. The speaker provided both tonal and white noise excitation of the array at a number of vehicle altitudes spanning 50 to 400 feet. The Mark I ACV was utilized at Fort A.P. Hill with multiple daily flights conducted to provide a running measure of sensor response.

The Mark II ACV consisted of a DJI S1000 Octo Flyer with the same MiniVox speaker and MP3 player as the Mark I vehicle. The Mark II ACV, shown in flight in Figure 42, incorporated retractable landing rails (to eliminate acoustic scattering from the rails) and the ability to lift heavier payloads. A significant enhancement to the Mark II vehicle was the addition of a Real Time Kinematic (RTK), Global Positioning System (GPS) allowing three-axis vehicle location data to be obtained relative to the phased array center and accurate to 0.4 inches. Note that a modification to the MiniVox speaker housing was also implemented on the Mark II vehicle. This modification involved the replacement of the original bezel cover over the paper-cone speaker with a 3D-printed open cover. As will be shown, the modification eliminated sound scattering by the bezel.

9.2 Ground Sound Sources

In addition to the aerial sound source, a new complementary calibration method for response tracking was attempted during the Edwards AFB deployment. The method consisted of embedding ground calibration speakers within the array and using these as fixed reference sound sources at precisely known locations. Several types of speakers were evaluated for their suitability for use as sound sources including horn drivers and domes. After testing several candidates, the Tymphany® BC25SC06 domed tweeter was chosen as the source since it exhibits the best output levels with minimal distortion and with an omnidirectional response. Note that a further benefit of using a domed tweeter is that the speaker can be easily flush-mounted into the same type of ground plates used to house the array microphones. An example of one of the speakers mounted in a ground plate can be seen in Figure 43.

Figure 43. Tweeter mounted on ground plate. [Source: NASA]

Figure 44. Risk-reduction testing of ground speakers. [Source: NASA]

Based on risk-reduction outdoor testing conducted at LaRC prior to the Edwards deployment (Figure 44), it was determined that acceptable time histories could be acquired by the array microphones under quiescent conditions up to 80 feet away from one of the ground sources when excited by a 2-kHz tone. Accordingly, eight speakers were strategically placed in a circular pattern halfway between the center and outer edge of the Edwards AFB array pattern. Speaker locations are depicted in Figure 45 (viewed from "behind" the array looking up).

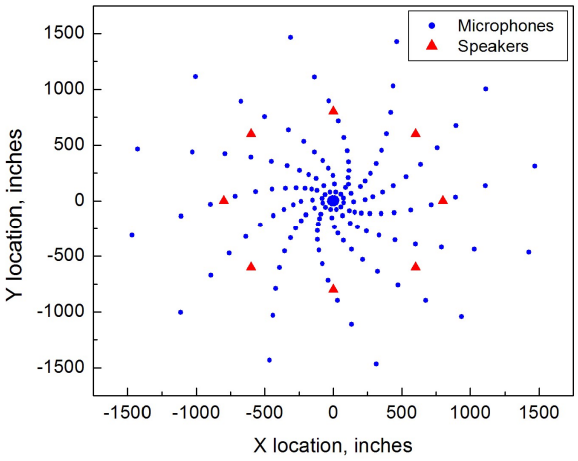

Figure 45. Array microphone and ground speaker locations for Edwards AFB array.

To provide sensor response tracking, each speaker was energized in turn with a 2-kHz tone with sufficient output power to excite the sensors without causing harmonic distortion in the speaker's output. Figure 46 shows typical ground footprints of local SPL levels for the speakers. The microphones excited by each speaker are denoted in the figure. Note that the 49 microphones in the central portion of the array (mounted on a common central mounting plate) are within 80 feet of all the speakers and thus are included in all calibration runs. In general, the footprints are very consistent for the various

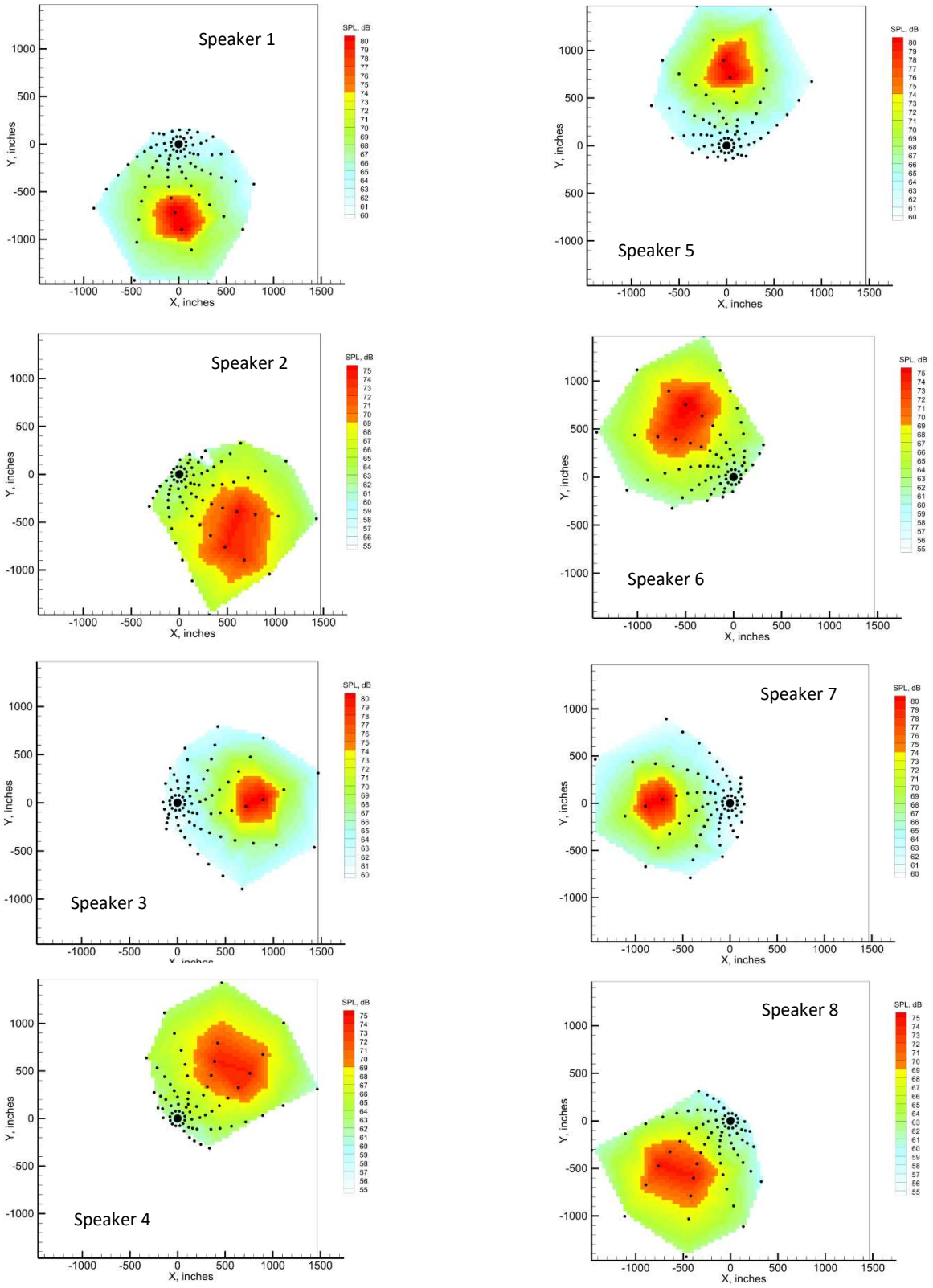

Figure 46. Nominal signal footprints for ground calibration speakers. The array microphones tracked by each speaker are shown.

speakers, with the footprints for speakers 1, 3, 5, and 7 located on the x and y axes of the array being slightly

more compact due to their closer proximity to the array microphones (resulting in higher recorded SPL levels on the order of 5 dB).

Proper tracking of microphone responses using either aerial or ground source methods requires a number of corrections to be performed to the recorded microphone outputs. These corrections include accounting for the effects of the speaker directivity as a function of propagation angle and frequency, atmospheric attenuation and the dB loss of sound from spherical spreading between the source and each microphone. These corrections are described in this section.

Corrections for Speaker Directivity: As described in [44], detailed characterizations of the aerial speakers utilized during the A.P. Hill and Edwards AFB deployments were performed in the LaRC Structural Acoustics Loads and Transmission (SALT) facility. Polar and azimuthal directivities as a function of frequency were measured for both the original speaker utilized on the Mark I ACV and the modified speaker utilized on the Mark II vehicle. Figure 47 shows the directivity functions for the two speaker configurations. As expected, removal of the bezel from the front of the Mark II ACV speaker resulted in a significant improvement in the structure of the directivity pattern at higher frequencies as seen in Figures 47(c) and 47(d).

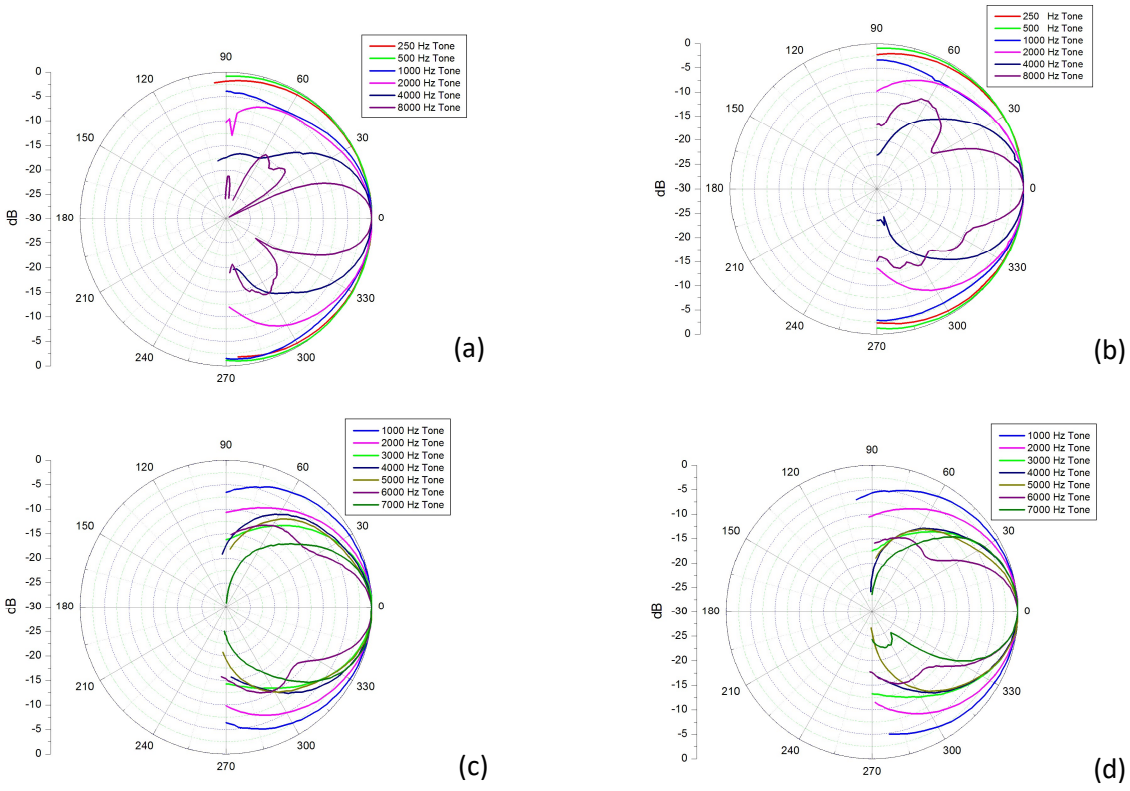

Figure 47. Aerial sound source directivity characteristics.
Polar (a) and azimuthal (b) directivity functions for Mark I ACV speaker.
Polar (c) and azimuthal (d) directivity functions for Mark II ACV speaker.

To predict the effects of speaker directivity on measured sound pressure levels given the small array aperture deployed at A.P. Hill and the much larger one deployed at Edwards, the maximum dB loss at those angles corresponding to the edges of the aperture in the polar and azimuthal directions were extracted from the functions in Figure 47 and tabulated in Table 3. Similar to the analysis shown in [44], the diameter of the array deployed at A.P. Hill was defined as 79 feet while the diameter of the Edwards array was defined as 250 feet. The vehicle altitudes were 400 and 350 feet for the ACV I and II vehicles, respectively.

Table 3. Predicted dB Losses at Edge of Array Due to Sound Source Directivity

	Mark I ACV Original Speaker		**Mark II ACV Modified Speaker**	
	Aperture = 79 feet, Altitude = 400 feet		**Aperture = 250 feet, Altitude = 350 feet**	
Frequency (Hz)	**Polar dB Loss**	**Azimuthal dB Loss**	**Polar dB Loss**	**Azimuthal dB Loss**
1000	0.1	0.2	0.4	0.4
2000	0.2	0.2	1.0	0.8
4000	0.3	0.1	1.9	1.6
7000	N/A	N/A	2.9	1.5
8000	0.6	0.6	N/A	N/A

An examination of the loss figures in Table 3 reveals that operating the speaker with a 4-kHz tone represents a good compromise between maintaining a smooth directivity function and providing enough speaker output (based on the manufacturer's published frequency response), while helping to properly separate the speaker tone from the ACV vehicle noise. Thus, all of the tracking data shown in Section 9.3 for the Mark I and II aerial sources were obtained using a 4-kHz tone. As seen in Figure 47, there is very little difference between the directivity functions in the polar and azimuthal directions at this frequency. Thus, a simplified approach was taken for computing a correction where it was assumed that the overall directivity function was hemispherical in structure. Thus, for individual microphones, the mean of the polar and azimuthal functions at a single directivity angle was used in computing an average ΔdB quantity to add to the microphone output:

$$\Delta dB_i = \frac{P_\theta(\alpha_i) + P_\varphi(\alpha_i)}{2}$$

$$\alpha_i = sin^{-1}(\frac{r}{d}) \tag{6}$$

where P_θ is the polar directivity function as shown in Figure 47, P_φ is the azimuthal directivity function, α_i is the directivity angle for the i^{th} microphone in the array, r is the distance from the microphone to the spot on the ground directly under the ACV (as reported by the on-board GPS tracking), and d is the line-of-sight distance from the aerial source to the microphone.

Although it was not measured in the LaRC SALT facility, it was assumed that the 90-degree polar and azimuthal directivity functions for the Tymphany tweeter ground speakers at Edwards were uniform based on manufacturer's response data for these devices. Given that the speakers are placed flat on the ground and incorporate a hemispherical dome diaphragm, it is safe to assume that the directivity should be omnidirectional to all of the microphones in the array within an 80-foot radius to the speaker. Thus, no corrections for directivity were performed for these speakers.

9.2 Health Monitoring Strategy

The overall strategy for tracking the response of individual microphones in the array was to establish an initial baseline output for each sensor. Deviations from this baseline were then identified via subsequent calibration runs using a combination of aerial and ground sound sources. If a microphone needed to be replaced in the array, then a new baseline was established at that point in time for the replaced sensor. The following procedures were developed to acquire time history data from the array in order to subsequently identify microphone response deviations from baseline levels and/or sensor or channel failures (occurring at any point in the sensor / data acquisition chain):

Aerial Sources

1. The sound source on the ACV was programmed to produce a 4-kHz tone and the vehicle was launched, centered over the array, and brought to the designated altitude (either 400 feet at A.P. Hill or 350 feet at Edwards AFB).
2. Time history data were captured for all of the array microphones over a nominal 10-second recording cycle.
3. For the initial run, the pressure squared values for each microphone were computed at a 4-kHz narrowband frequency and the equivalent sound pressure level (SPL) was calculated. Full corrections for speaker directivity and atmospheric attenuation as described previously were applied to the SPL values. This defined the baseline SPL for each microphone.
4. Absolute output changes across the array due to speaker drift as a function of time must be taken into account. Thus, for subsequent aerial source runs, the current microphone outputs had a reference level, dB_{ref}, subtracted from them. dB_{ref} was obtained via one of two methods depending on the location of a microphone in the array: (1) for those sensors located within 24 feet of the center of the array, a mean dB was computed for the inner 49 microphones in the array with dB_{ref} defined as the difference between the means for the current and baseline acquisitions, or (2) for those sensors located outside the 24-foot radius from the center, the mean was computed from the nearest 8 neighboring microphones, again with dB_{ref} defined as the difference between the means for the current and baseline acquisitions.
5. Each subsequent calibration produced a ΔdB_{mic} by subtracting the baseline level from the current calibration via

$$\Delta dB_{mic} = (dB_{mic} - dB_{ref})_{calibration} - (dB_{mic} - dB_{ref})_{baseline} \quad (7)$$

   A running history of the ΔdB_{mic} levels was maintained to observe trends and track the microphone responses.

Ground Sources

1. Each of the 8 speakers embedded in the array pattern were excited individually using a 2-kHz tone.
2. For each speaker excitation, time history data was captured for all of the array microphones over a nominal 10-second recording cycle.
3. Baseline SPL levels and a running history of subsequent ΔdB_{mic} levels were obtained in the same manner as described previously in steps (3) – (5) for the aerial sources.

Two additional considerations needed to be addressed as part of the response tracking strategy. First, for the ground sources at Edwards, extreme changes in temperature encountered on the runway during the course of the deployment needed to be taken into account. Aeroacoustic flyover testing at Edwards normally commences around sunrise when the atmosphere is relatively calm. Testing continues until surface heating either reduces the humidity below a minimum threshold or the winds increase above a maximum threshold. During this period, the temperature at the surface can vary as much as 30 degrees F. This modifies the output of the ground speakers due to an effect known as speaker thermal compression [45]. As seen in Figure 48 with data obtained at Edwards on two different days, a significant drop in speaker SPL was observed as the temperature increased. It is difficult to correct for this effect; therefore, tracking of microphone responses using the ground speakers was only performed for runs obtained at matched temperatures (i.e., normally the first run of the morning where temperatures were somewhat uniform day to day). Note that the aerial speakers utilized for calibration runs did not exhibit noticeable thermal effects due to better ventilation under the ACV which limited the heating of the speaker. The speakers on the runway surface were encased in ground plates without ventilation and thus experienced much higher temperatures.

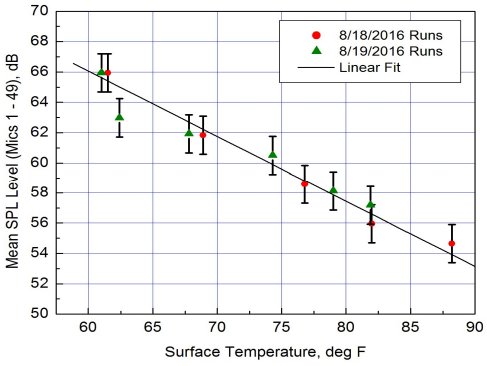

Figure 48. Effect of speaker thermal compression on observed output level. 95% confidence intervals shown.

The second consideration to be addressed concerned the effect of surface winds on the inter-channel coherence observed between microphone time histories for both aerial source and ground source calibration runs. An examination of multiple coherence functions revealed that the best tracking performance occurred for those runs exhibiting the highest consistent coherence between microphones. The high inter-channel coherence also correlated very well with lower average surface wind speeds (regardless of wind direction). Therefore, tracking of microphone responses for both aerial and ground source runs only occurred for those runs where the average wind speed did not exceed a defined maximum limit of 5 feet/sec.

9.3 Health Monitoring Examples

Fort A.P. Hill Aerial Source: The first example of microphone response tracking and array health monitoring occurred at Fort A.P. Hill for aerial sound source measurements obtained using the Mark I ACV. These are shown in Figures 49 and 50 for measurements conducted over a 7-day period where a total of 8 individual runs satisfied the tracking strategy given in Section 9.2. Sixteen representative microphones were selected for inclusion in these figures, with sensors taken from the following regions of the array aperture: (1) four microphones on the central mounting plate, (2) four microphones located near the central plate, (3) four microphones located midway along the starburst arms of the array, and (4) four microphones located at the outer limits of the aperture. These selected microphones spanned all four quadrants of the array. The ΔdB values for a particular sensor have been normalized by the baseline level taken from the first calibration run. The error bars represent 95% confidence intervals based on the identification of the spectral peaks in the auto-spectra used to generate the tracking data. All of the auto-spectra were generated using Welch's periodogram method [46].

As seen in Figures 49 and 50, the majority of the microphones in the array maintained fairly uniform output levels as a function of time during the deployment. However, a few sensors did exhibit problems. In particular, microphone #93 (Figure 50(e)) showed a marked 3dB drop in output after the first day of the deployment. This is characteristic of a partial sensor failure, and although this sensor was not replaced in the array during the A.P. Hill deployment, the drop in output shown by the tracking data would be sufficient justification for such a replacement. Similarly, microphone #3 (Figure 49(b)) and microphone #125

(Figure 50(b)) showed drops in output toward the end of the deployment that might be indicative of partial sensor failures as well. A couple microphones displayed some variability in the tracking (microphone #185 in particular in Figure 50(h)); however, it is not as apparent from this data whether there were any problems occurring with these sensors. In general, the aerial sound source calibrations worked very well during the A.P. Hill deployment.

Edwards AFB Ground Sources: The second example of tracking the array response and health occurred at Edwards AFB for ground source measurements obtained over a period from August 18 – October 5, 2016. During this time, a total of 13 individual runs satisfied the tracking strategy given in Section 9.2 (i.e., matched temperatures and wind speeds below 5 feet/sec). In a similar approach to that shown for the Fort A.P. Hill data, sixteen representative microphones were selected from the array aperture covering both inner, middle, and outer portions of the aperture across all four quadrants. These selected microphones are shown in Figures 51 and 52. The speaker used to excite the microphone is denoted on each figure. Note that gaps appearing in the tracking data in individual figure panels represent outliers that were identified and removed using a modified Thompson-tau method [47].

In general, the ground source calibrations did a good job of providing response tracking information for the array sensors. Most of the microphones in Figures 51 and 52 show only a minimal drift in response over the almost two-month period they were deployed at Edwards in a relatively harsh environment (e.g., dust, high heat, wildlife intrusion, etc.). A couple microphones (#108 and #106) did exhibit an approximate +2dB drift toward the end of the deployment. Although not shown in the figures, a few failed sensors were identified from their response tracking during the course of the deployment and replaced.

An interesting observation was that the day to day variability in the tracking was more pronounced for those sensors located near the edge of the array aperture versus those situated near the center of the array. Indeed, the majority of outliers removed from the data occurred for those microphones in the middle to outer portions of the array. The reason for the increased variability in tracking in the outer regions of the array aperture is not well understood yet. It is speculated that ground scattering effects may create variable sound propagations to individual microphones. Also, there may be deviations from the assumed uniform 90-degree directivity function as the sound propagates from the speakers to the individual microphones.

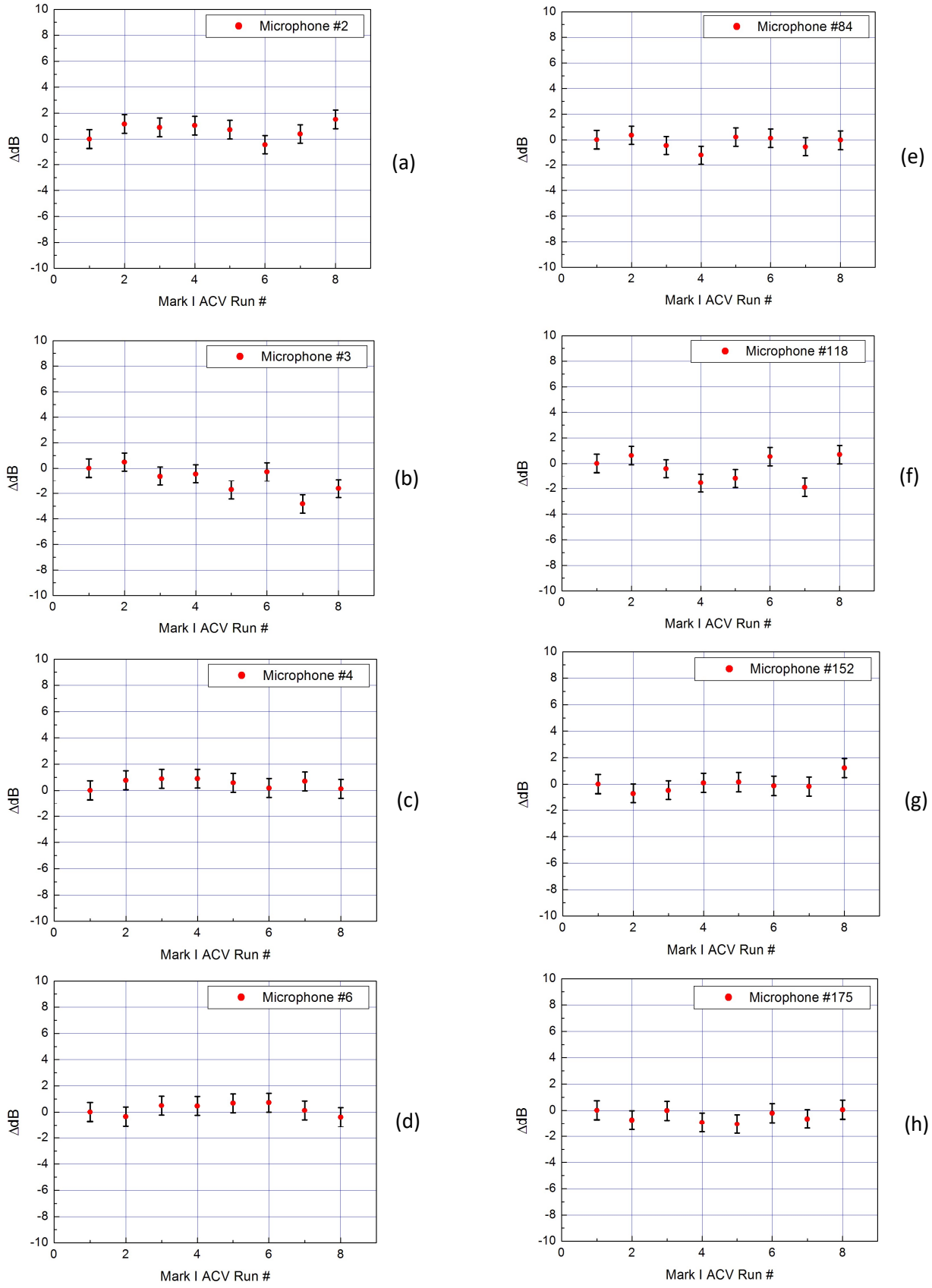

Figure 49. Tracking of measured microphones levels for 8 separate Mark I ACV runs conducted at Fort A.P. Hill over a 7-day period spanning August 27 – September 3, 2015.

(a) – (d) are microphones on central plate, (e) – (h) are individual inner microphones

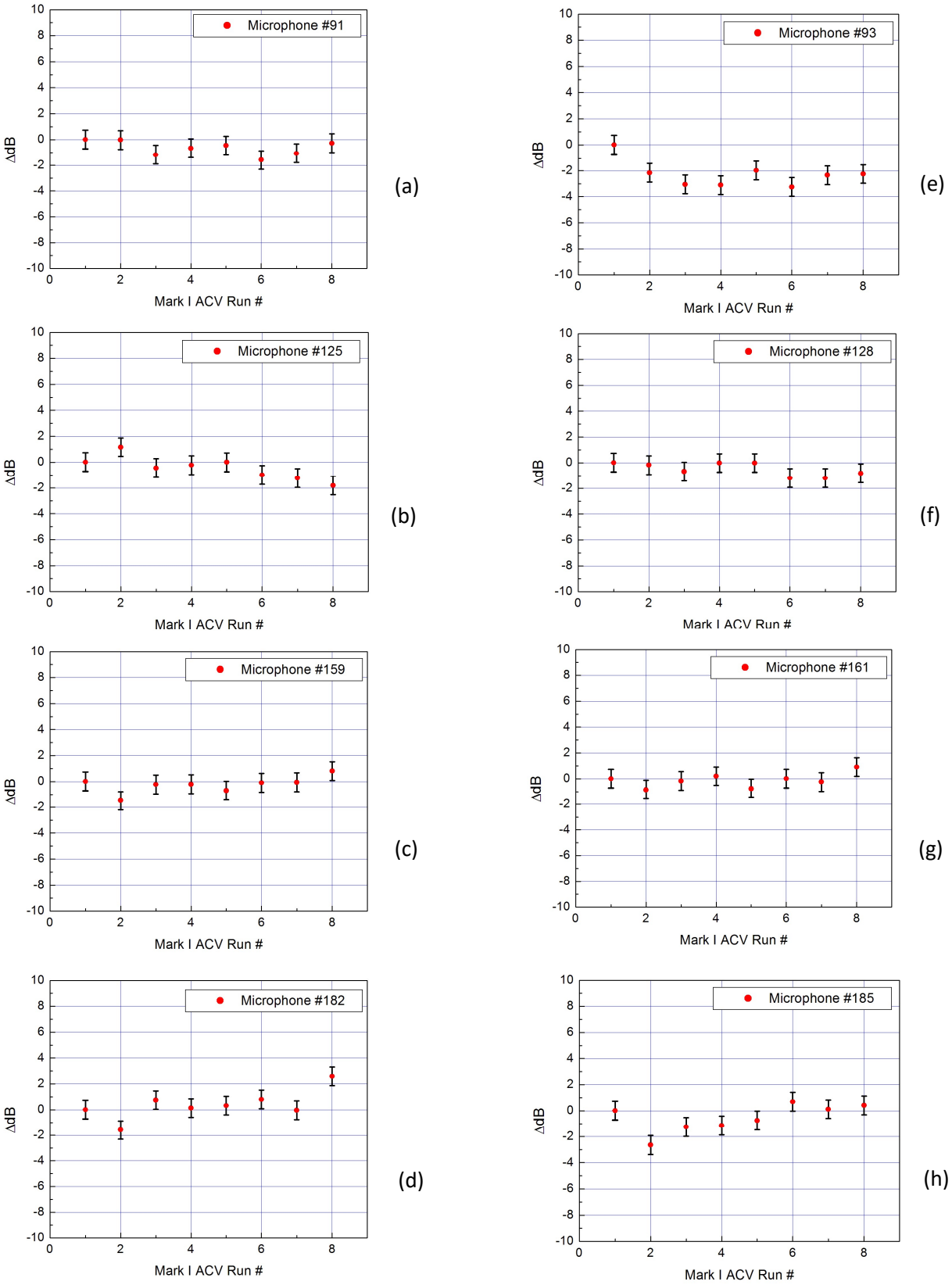

Figure 50. Tracking of measured microphones levels for 8 separate Mark I ACV runs conducted at Fort A.P. Hill over a 7-day period spanning August 27 – September 3, 2015.

(a) – (d) are individual middle microphones, (e) – (h) are individual outer microphones

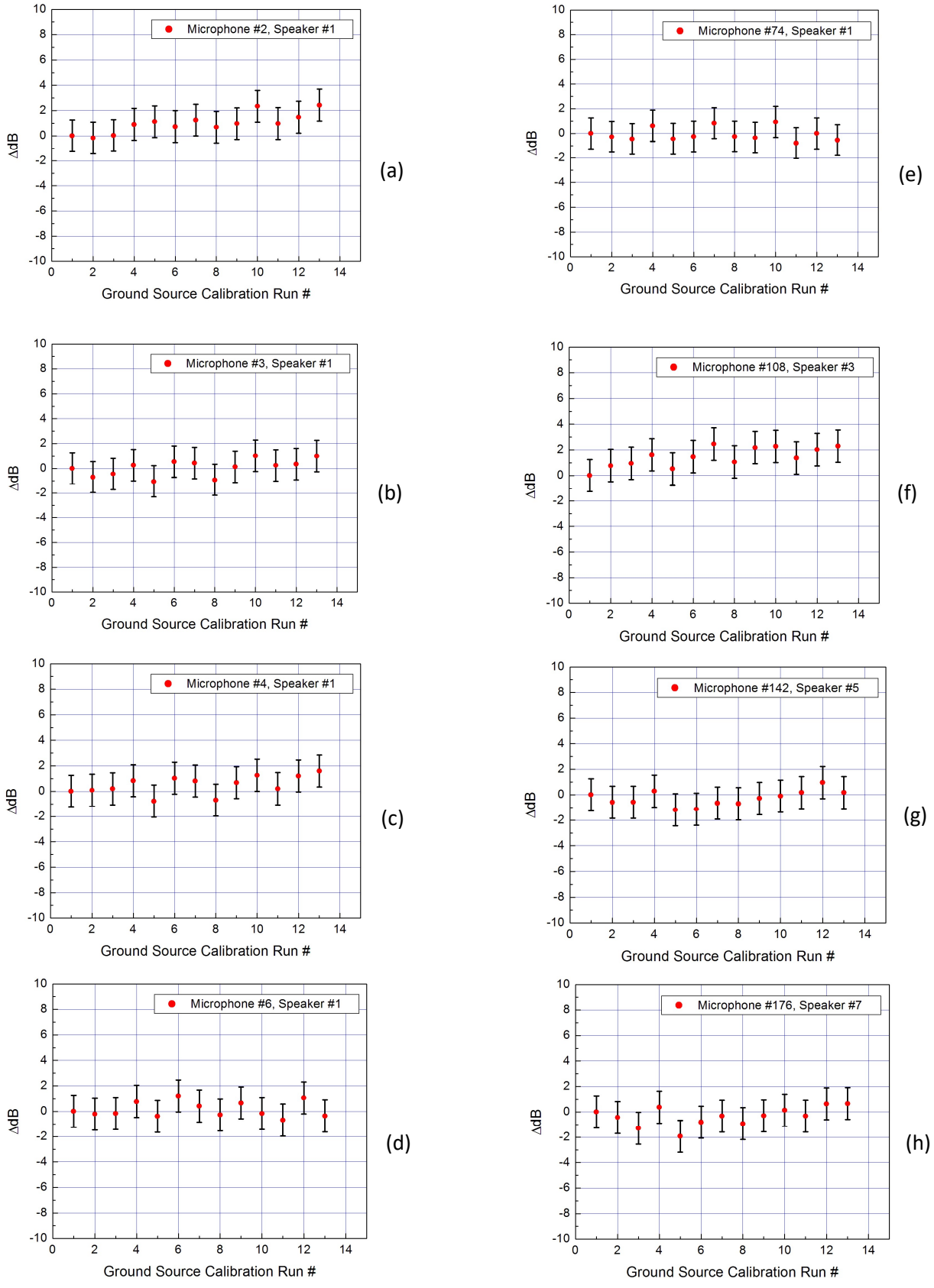

Figure 51. Tracking of measured microphone levels for 13 separate ground source runs conducted at Edwards AFB from August 18 – October 5, 2016.

(a) – (d) are microphones on central plate, (e) – (h) are individual inner microphones

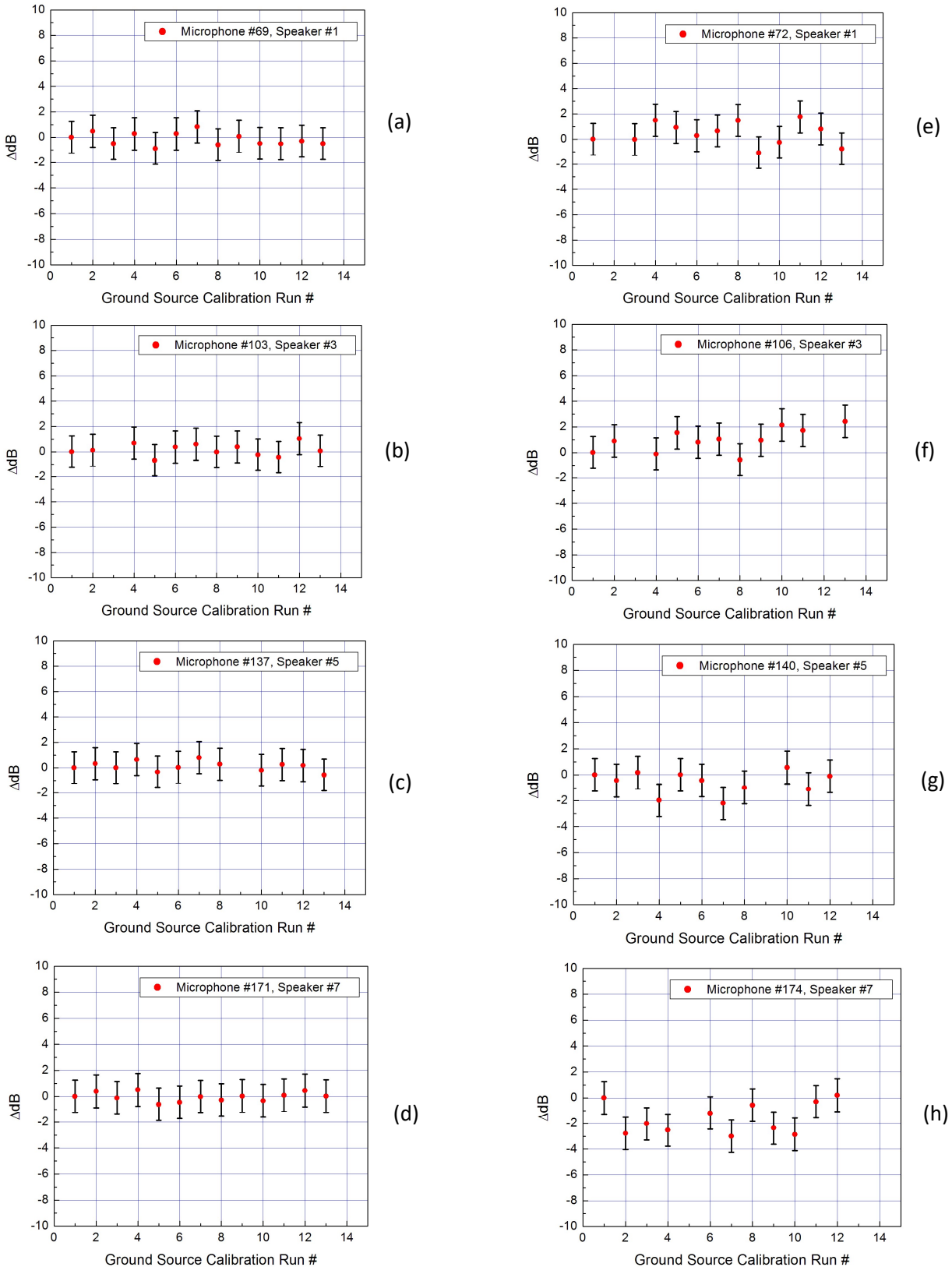

Figure 52. Tracking of measured microphone levels for 13 separate ground source runs conducted at Edwards AFB from August 18 – October 5, 2016.

(a) – (d) are individual middle microphones, (e) – (h) are individual outer microphones

Edwards AFB Aerial Sources: A final example of tracking array microphone response also occurred at Edwards, using Mark II ACV aerial sound source calibrations conducted from August 18 – October 4, 2016. During this time, a total of 12 individual runs both satisfied the tracking strategy described in Section 9.2 (i.e., wind speeds below 5 feet/sec) and matched same-day ground speaker runs so that comparisons between the two methods could be performed. The aerial sound source results are shown in Figures 53 and 54. The representative microphones selected from the array are the same as those shown in Figures 49 and 50. Outliers in the tracking data were identified and removed.

In general, the Mark II aerial source did a reasonable job of providing response tracking information for the array sensors, although the uniformity in the data is not as good as that shown in Figures 49 and 50 for the A.P. Hill aerial source calibrations. There was more variability in the tracking response in particular in Figure 54 for those microphones located in the middle and outer portions of the array aperture. This was not necessarily surprising given the large solid angle subtended by the array (39.3 degrees) with the ACV at an altitude of 350 feet. The propagation distances to the outer microphones were significantly longer than those for sensors near the center of the array, requiring larger corrections for directivity and atmospheric absorption. Any additional factors influencing the sound propagation beyond those assumed in the corrections will diminish the effectiveness of those corrections.

One effect that has not been investigated in detail to date is the ACV rotor downwash affecting the propagation of sound through the ensuing shear layer under the vehicle. The Mark I ACV was a smaller, lighter vehicle (see Table 2), and thus exhibited less thrust from individual rotors with a corresponding decrease in the strength of the downwash. Coupled with the much smaller array aperture utilized at Fort A.P. Hill (where the microphones were more centrally located under the vehicle) this could account for the better tracking performance shown in Figures 49 and 50. Some evidence for the effect of array size coupled with ACV rotor downwash can be seen in Figure 55 where two ground footprint noise contours for representative Mark I and Mark II ACV runs are shown. These footprints were obtained via a linear interpolation of the levels recorded by the microphones at a frequency of 4 kHz, projected onto a uniformly-spaced Cartesian grid. For reference, the black circle in Figure 55(b) denotes the perimeter of the A.P. Hill array aperture superimposed on the much larger aperture used at Edwards. The uniformity of the footprint for the smaller array aperture is clearly shown in Figure 55(a). This is contrasted with the contours shown in Figure 55(b) where partial uniformity is observed only near the center of the array. More work is needed to understand the full effects of the vehicle aerodynamics on the fidelity of measuring the sound generated by the aerial sound source.

Comparison of Methods: Figure 56 shows a comparison of tracking performance between the aerial and ground source methods conducted at Edwards. Four representative microphones are shown taken individually from the central plate and the inner, middle, and outer regions of the array aperture. For clarity, the 95% confidence intervals are only shown for the aerial source data; however, the error bars are of a similar size for the ground source data. It is immediately apparent from an examination of the data that almost perfect agreement in the tracking is observed for the microphone on the array central plate. As one moves to microphones farther away from the center of the array, the agreement between the two calibration methods degrades but is still quite good for the majority of the runs shown when taking into account the overlap in the 95% confidence intervals for the data. There are some periods, for instance in runs 6 through 9 in Figure 56(c), where significant deviations are shown between the two methods. However, these deviations decrease (at least for this microphone) toward the end of the displayed runs. It can be concluded from this comparison of methods that no one calibration technique is perfect when working under the sometimes harsh ambient conditions that field-deployed arrays and calibration systems are exposed. Therefore, the use of multiple response tracking methods like the two described herein is justified in order to allow better decisions to be made during a deployment regarding the health of the individual array sensors.

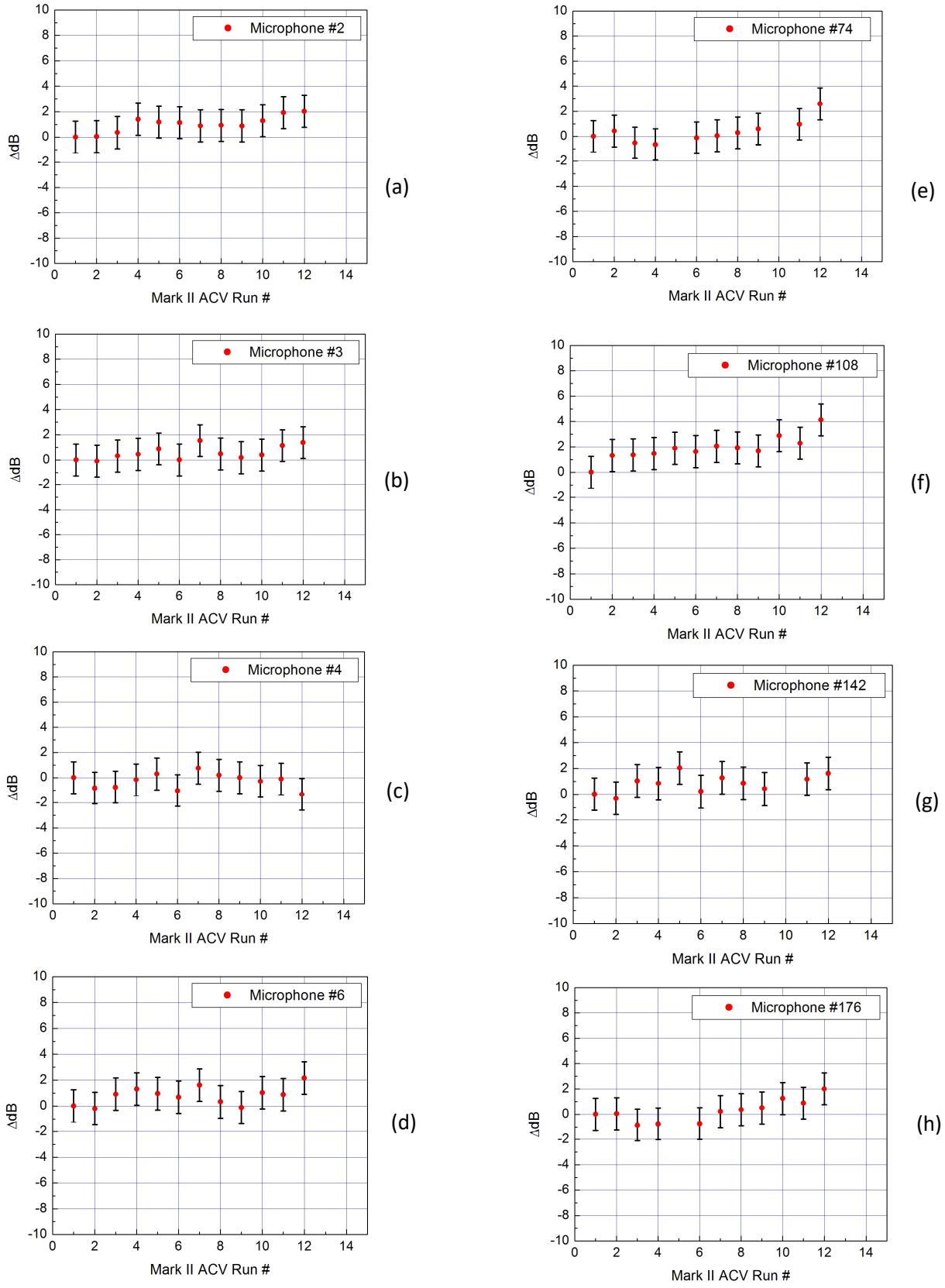

Figure 53. Tracking of measured microphone levels for 12 separate Mark II ACV runs conducted at Edwards AFB from August 18 – October 5, 2016.
(a) – (d) are microphones on central plate, (e) – (h) are individual inner microphones

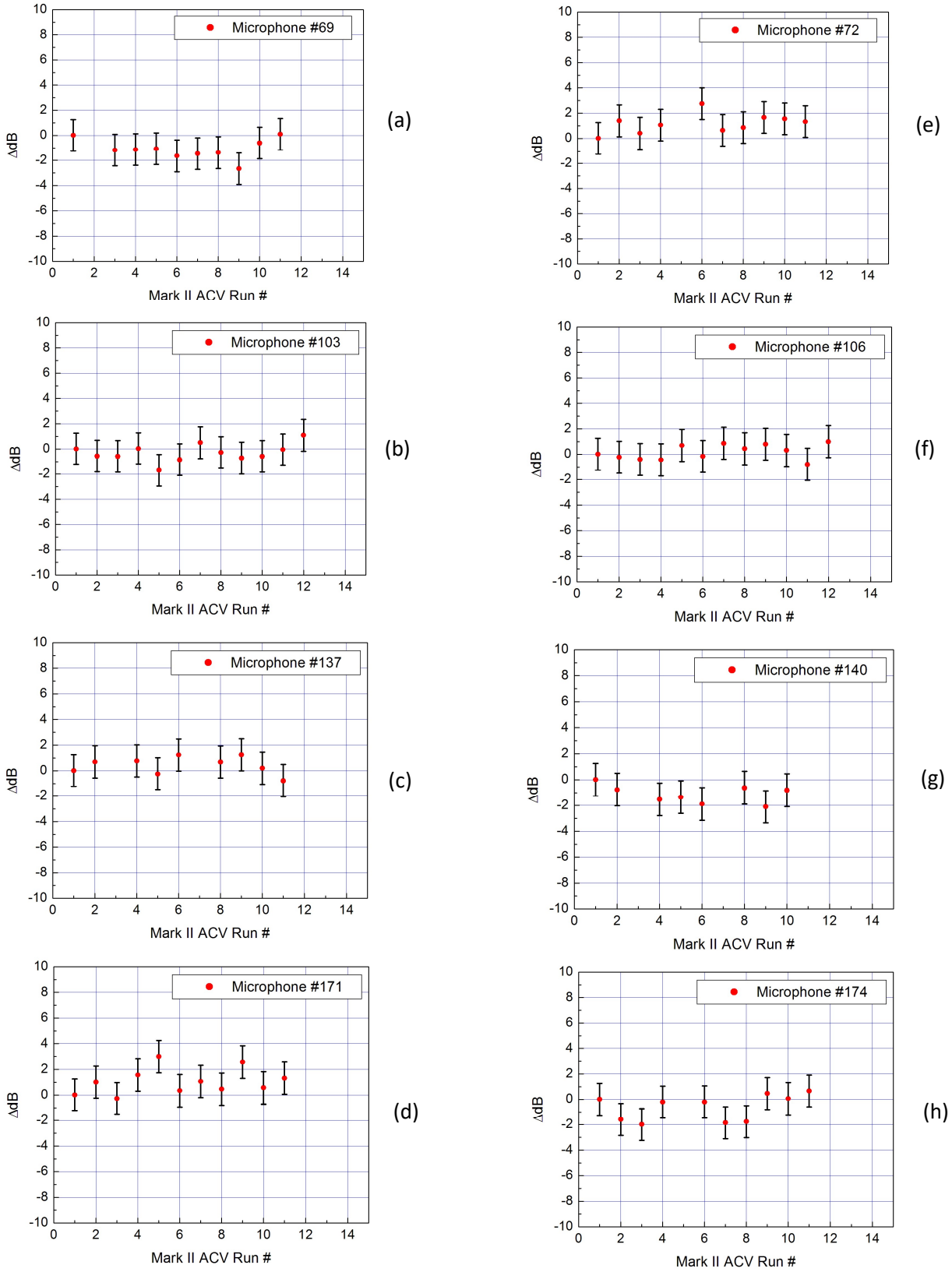

Figure 54. Tracking of measured microphone levels for 12 separate Mark II ACV runs conducted at Edwards AFB from August 18 – October 5, 2016.

(a) – (d) are individual middle microphones, (e) – (h) are individual outer microphones

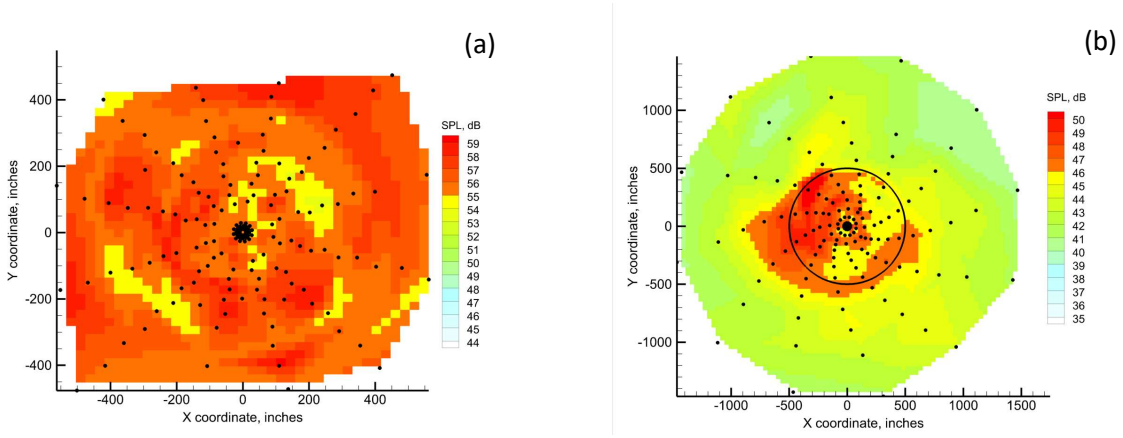

Figure 55. Representative 4-kHz noise footprints for ACV flights.
(a) Mark I ACV, Fort A.P. Hill, altitude = 400 feet
(b) Mark II ACV, Edwards, altitude = 350 feet

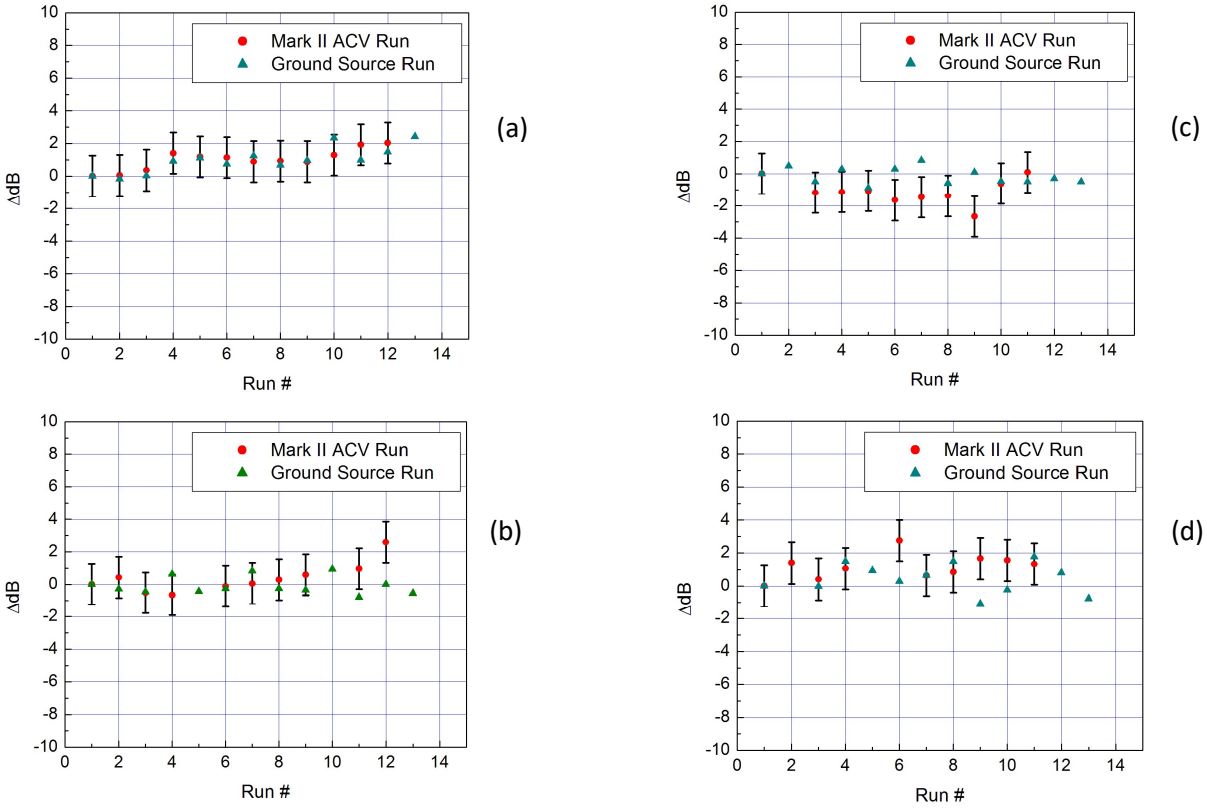

Figure 56. Comparison of tracking performance between ground source and Mark II ACV runs conducted at Edwards AFB from August 18 – October 5, 2016.

(a) central plate microphone #2, (b) inner microphone #74,
(c) middle microphone #69, (d) outer microphone #72

10.0 Summary and Lessons Learned

A new aeroacoustic measurement capability was developed for use in measurement of airframe and propulsive noise for a range of aircraft types and scales. The instrumentation consisted of a large channel-count, field-deployable microphone phased array plus support hardware. The array incorporated up to 185 hardened, weather-resistant sensors suitable for extended outdoor deployment. A custom 4-mA current loop receiver circuit with temperature compensation was developed to power the sensors over extended cable lengths with minimal degradation of the signal to noise ratio and frequency response. A compact data system combining sensor power, signal conditioning, and digitization was assembled for use with the array, as were a commercial weather station and a video monitoring / recording system. The array system was thoroughly tested in the Langley Acoustic Development Laboratory prior to deployments at Fort A.P. Hill to measure the noise generated by a range of sUAS aircraft and at Edwards AFB to measure airframe noise on full-scale transport aircraft during a 3-year flight test campaign. During these deployments, new array health monitoring methods using a hovering aerial sound source and ground speakers were attempted for the first time. The results indicated that daily drifts in microphone sensitivities could be tracked and failing sensors easily identified. In general, the array operation during the deployments described in this report was nominal with remarkable stability observed for the microphones, and the array performed as designed.

Lessons learned: The advantage of having performed shakedown testing as well as multiple deployments of the array is that numerous lessons are learned that can be of benefit to future array deployments. Some of the many lessons learned from the development and deployment of the array described in this report are:

1. It is critical to eliminate as many single points of failure as possible in the overall array sensor and data systems. This can be accomplished by having backup hardware on hand, although this can increase the overall cost of the deployment. For example, during the ARM-III test campaign, systemic failures were observed on many of the primary signal conditioning channels for reasons that were never determined (it was speculated that environmental conditions during hardware storage was a cause). Nevertheless, a backup strategy was available using alternate signal conditioning that saved the flight test. Similarly, loss of the Solid State Drive (SSD) boot disk in the primary acquisition computer did not result in a work stoppage since an imaged backup was available.
2. Cold weather operation can be an issue, especially with data system hardware and aerial sound source components. Experience during the ARM test campaigns indicated that cold weather operation doesn't become an acute issue until the temperature drops below 40 degrees F.
3. High moisture operation of the array can be an issue. There were unexpected moisture issues with the array during the ARM-III campaign that did not occur during ARM-I or ARM-II given that the latter deployments were conducted during the dry season at Edwards AFB. In particular, the conformal coating of the microphones was not totally effective when 100% humidity and dew were present in pre-dawn array start-up periods, implying that an improved method of coating should be used. Also, despite the fact that the microphones used in the array were waterproof, moisture could still intrude into the pinholes leading to the diaphragm thereby affecting the sensor response until the moisture could be driven out of the devices.
4. Better understanding and considerations of ACV vehicle weight, number of rotors, and the location of the sound source in relation to the downwash are needed to minimize the variability in microphone health monitoring when using an aerial sound source.

11.0 Acknowledgments

The authors gratefully acknowledge the support and expertise of the NASA Langley and NASA Armstrong UAS Operations Offices in coordinating the sUAS testing conducted at Fort A.P. Hill and Edwards AFB. The authors also gratefully acknowledge the support of personnel at the NASA Armstrong Flight Research Center in the coordination and set up of the array hardware at Edwards AFB. This work was funded by the NASA Environmentally Responsible Aviation (ERA) Project under Integrated Technology Demonstration activity (ITD) 50A and by the NASA Flight Demonstrations and Capabilities (FDC) Project.

12.0 References

[1] Collier, F. S., "Environmentally Responsible Aviation (ERA) Project," oral presentation, NASA Fundamental Aeronautics Program, Third Annual Meeting, Atlanta, GA, September, 2009.

[2] Khorrami, M. R., Humphreys, W. M., Jr., Lockard, D. P., and Ravetta, P. A., "Aeroacoustic Evaluation of Flap and Landing Gear Noise Reduction Concepts,", AIAA Paper 2014-2478, 20th AIAA/CEAS Aeroacoustics Conference, Atlanta, GA, 2014. https://doi.org/10.2514/6.2014-2478

[3] Elliot, R.S., "The Theory of Antenna Arrays," *Microwave Scanning Antennas*, R.C. Hansen, ed., Academic Press, 1966.

[4] Burdic, W.S., *Underwater Acoustic System Analysis*, Prentice-Hall, Inc., Englewood Cliffs, NJ, 1984.

[5] Soderman, P.T., and Noble, S.C., "A Four-Element End-Fire Microphone Array for Acoustic Measurements in Wind Tunnels," *NASA Technical Memorandum X-62*, 331, January, 1974.

[6] Soderman, P.T., and Noble, S.C., "Directional Microphone Array for Acoustic Studies of Wind Tunnel Models," *Journal of Aircraft*, Vol. 12, No. 3, pp. 169-173, 1975. https://doi.org/10.2514/3.59813

[7] Billingsley, J., and Kinns, R., "The Acoustic Telescope," *Journal of Sound and Vibration*, Volume 48, Number 4, pp. 485-510, 1976. https://doi.org/10.1016/0022-460X(76)90552-6

[8] Brooks, T.F., Marcolini, M.A., and Pope, D.S., "A Directional Array Approach for the Measurement of Rotor Noise Source Distributions with Controlled Spatial Resolution," *Journal of Sound and Vibration*, Vol. 112, No. 1, pp. 192-197, 1987. https://doi.org/10.1016/S0022-460X(87)80105-0

[9] Marcolini, M.A., and Brooks, T.F., "Rotor Noise Measurement Using a Directional Microphone Array," *Journal of the American Helicopter Society*, pp. 11-22, 1992. https://doi.org/10.4050/JAHS.37.11

[10] Underbrink, J.R., "Practical Considerations in Focused Array Design for Passive Broadband Source Mapping Applications," *Master's Thesis*, The Pennsylvania State University, May, 1995.

[11] Mosher, M., "Phased Arrays for Aeroacoustic Testing: Theoretical Development," AIAA Paper 1996-1713, 2nd AIAA/CEAS Aeroacoustics Conference, State College, PA, May, 1996. https://doi.org/10.2514/6.1996-1713

[12] Watts, M.E., Mosher, M., and Barnes, M.J., "The Microphone Array Phased Processing System (MAPPS)," AIAA Paper 1996-1714, 2nd AIAA/CEAS Aeroacoustics Conference, State College, PA, May, 1996. https://doi.org/10.2514/6.1996-1714

[13] Humphreys, W. M., Jr., Brooks, T. F., Hunter, W. W., Jr., and Meadows, K. R., "Design and Use of Microphone Directional Arrays for Aeroacoustic Measurements," AIAA Paper 1998-0471, 36st Aerospace Sciences Meeting and Exhibit, Reno, NV, 1998. https://doi.org/10.2514/6.1998-471

[14] Johnson, D. H, and Dudgeon, D. E., *Array Signal Processing: Concepts and Techniques*, Prentice Hall, 1993.

[15] Brooks, T. F., and Humphreys, W. M., Jr., "A Deconvolution Approach for the Mapping of Acoustic Sources (DAMAS) Determined from Phased Microphone Arrays," *Journal of Sound and Vibration*, Vol. 294, pp. 856-879, 2006. https://doi.org/10.1016/j.jsv.2005.12.046

[16] Dougherty, R. P., "Extensions of DAMAS and Benefits and Limitations of Deconvolution in Beamforming," AIAA Paper 2005-2961, 11th AIAA/CEAS Aeroacoustics Conference, Monterey, CA, 2005. https://doi.org/10.2514/6.2005-2961

[17] Suzuki, T., "L1 Generalized Inverse Beamforming Algorithm Resolving Coherent/Incoherent, Distributed, and Multipole Sources," *Journal of Sound and Vibration*, Volume 330, Number 24, pp. 5835-5851, 2011. https://doi.org/10.1016/j.jsv.2011.05.021

[18] Dougherty, R.P., "Enhancing Deconvolution with Functional Beamforming," BeBeC-2022-S01, 2022 Berlin Beamforming Conference, Berlin, Germany, June 2022.

[19] Merino-Martinez, R., Sijtsma, P., Snellen, M., et al., "A Review of Acoustic Imaging Methods Using Phased Microphone Arrays," *CEAS Aeronautical Journal*, Vol. 10, No. 197, March, 2019. https://doi.org/10.1007/s13272-019-00383-4

[20] Underbrink, J. R., "Aeroacoustic Phased Array Testing in Low Speed Wind Tunnels," In: Mueller, T. J. (editor) *Aeroacoustic Measurements*, Experimental Fluid Mechanics, Springer, 2002. https://doi.org/10.1007/978-3-662-05058-3

[21] Underbrink, J. R., "Pletharrays for Aeroacoustic Phased Array Applications," AIAA Paper 2015-2978, 21st AIAA/CEAS Aeroacoustics Conference, Dallas, TX, 2015. https://doi.org/10.2514/6.2015-2978

[22] Michel, U., Barsikow, B., Haverich, B., and Schüttpelz, M., "Investigation of Airframe and Jet Noise in High-Speed Flight with a Microphone Array," AIAA Paper 1997-1596, 3rd AIAA/CEAS Aeroacoustics Conference, Atlanta, GA, 1997. https://doi.org/10.2514/6.1997-1596

[23] Michel, U., Barsikow, B., Helbig, J., Hellmig, M., and Schüttpelz, M., "Flyover Noise Measurements on Landing Aircraft with a Microphone Array," AIAA Paper 1998-2336, 4th AIAA/CEAS Aeroacoustics Conference, Toulouse, France, 1998. https://doi.org/10.2514/6.1998-2336

[24] Ulf, M., and Qiao, Weiyang, "Directivity of Landing-Gear Noise Based on Flyover Measurements," AIAA Paper 1999-1956, 5th AIAA/CEAS Aeroacoustics Conference, Bellevue, CA, 1999. https://doi.org/10.2514/6.1999-1956

[25] Piet, J. F., Elias, G., and Lebigot, P., "Localization of Acoustic Source from a Landing Aircraft with a Microphone Array," AIAA Paper 1999-1811, 5th AIAA/CEAS Aeroacoustics Conference, Bellevue, CA, 1999. https://doi.org/10.2514/6.1999-1811

[26] Piet, J. F., Michel, U., and Bohning, P., "Localization of the Acoustic Sources of the A340 with a Large Phased Microphone Array During Flight Tests," AIAA Paper 2002-2506, 8th AIAA/CEAS Aeroacoustics Conference, Breckenridge, CO, 2002. https://doi.org/10.2514/6.2002-2506

[27] Czech, M. J., Thomas, R. H., Guo, Y., June, J. C., Clark, I. A., and Shoemaker, C. M., "Propulsion Airframe Aeroacoustics and Aircraft System Noise Flight Test on the Boeing 2020 ecoDemonstrator Program," AIAA Paper 2022-2994, 28th AIAA/CEAS Aeroacoustics Conference, Southampton, UK, 2022. https://doi.org/10.2514/6.2022-2994

[28] Brusniak, L., Underbrink, J. and Stoker, R., "Acoustic Imaging of Aircraft Noise Sources Using Large Aperture Phased Arrays," AIAA Paper 2006-2715, 12th AIAA/CEAS Aeroacoustics Conference, Cambridge, MA, 2006. https://doi.org/10.2514/6.2006-2715

[29] Khorrami, M. R., Lockard, D. P., Humphreys, W. M., Jr., Choudhari, M. M., and Van de Ven, T., "Preliminary Analysis of Acoustic Measurements from the NASA-Gulfstream Airframe Noise Flight Test," AIAA Paper 2008-2814, 14th AIAA/CEAS Aeroacoustics Conference, Vancouver, Canada, 2008. https://doi.org/10.2514/6.2008-2814

[30] Guerin, S., Weckmuller, C., and Michel, U., "Beamforming and Deconvolution for Aerodynamic Sound Sources in Motion," Proceedings of the Berlin Beamforming Conference (BeBeC), Berlin, Germany, 2006.

[31] Dowling, A., "Convective Amplification of Real Simple Sources," *Journal of Fluid Mechanics*, Vol. 74, No. 3, pp. 529-546, 1976. https://doi.org/10.1017/S0022112076001936

[32] Crighton, D. G., Dowling, A. P., Williams, J. E. F., Heckl, M., and Leppington, F. G., "Effects of Motion on Acoustics Sources," In: *Modern Methods in Analytical Acoustics*, Springer, 1992. https://doi.org/10.1007/978-1-4471-0399-8_14

[33] Howell, G. P., Bradley, A. J., McCormick, M. A., and Brown, J. D., "De-Dopplerization and Acoustic Imaging of Aircraft Flyover Noise Measurements," *Journal of Sound and Vibration*, Vol. 105, No. 1, pp. 151 – 167, 1986. https://doi.org/10.1016/0022-460X(86)90227-0

[34] Dougherty, R., "Advanced Time-Domain Beamforming Techniques," AIAA-2004-2955, 10th AIAA/CEAS Aeroacoustics Conference , Manchester, UK, May, 2004. https://doi.org/10.1016/0022-460X(86)90227-0

[35] True, H. C., "The Layered Weather Correction for Flyover Noise Testing," AIAA Paper 1976-0895, AIAA Aircraft Systems and Technology Meeting, Dallas, TX, 1976. https://doi.org/10.2514/6.1976-895

[36] ANSI Standard, "Method for the Calculation of the Absorption of Sound by the Atmosphere," ANSI S1.26-1978, American National Standards Institute, Inc., June, 1978.

[37] Sijtsma, P., "CLEAN Based on Spatial Source Coherence," AIAA-2007-3436, 13th AIAA/CEAS Aeroacoustics Conference, Rome, Italy, 2014. https://doi.org/10.2514/6.2007-3436

[38] Beranek, L. L., *Acoustical Measurements*, American Institute of Physics, 1993, pp. 643.

[39] Jones, D. C., "Microphone Phased Array Hardware Calibration and Software Development for Aeroacoustic Flight Testing," NASA Langley STEM Takes Flight Student Summary Report, 2018.

[40] Baumann, E. and Waggoner, E., "Flight and Ground Operations in Support of Airframe Noise Reduction Tests," 2018 AIAA/CEAS Aeroacoustics Conference, AIAA paper 2018-2970, 18th AIAA/CEAS Aeroacoustics Conference, Atlanta, GA, 2018. https://doi.org/10.2514/6.2018-2970

[41] Khorrami, M. R., Lockard, D. P., Humphreys, W. M. Jr., and Ravetta, P. A., "Flight-Test Evaluation of Airframe Noise Mitigation Technologies," AIAA paper 2018-2972, 18th AIAA/CEAS Aeroacoustics Conference, Atlanta, GA, 2018. https://doi.org/10.2514/6.2018-2970

[42] Khorrami, M. R., Lockard, D. P., Humphreys, W. M. Jr., and Ravetta, P. A., "Flight-Test Evaluation of Landing Gear Noise Reduction Technologies," AIAA paper 2019-2455, 25th AIAA/CEAS Aeroacoustics Conference, Delft, The Netherlands, 2019. https://doi.org/10.2514/6.2019-2455

[43] Dolph, C. V., McSwain, R. G., Humphreys, W. M., Jr., Lockard, D. P., and Khorrami, M. R., "Optical Geolocation for Small Unmanned Aerial System," AIAA Paper 2019-1055, AIAA SciTech Forum, San Diego, CA, 2019. https://doi.org/10.2514/6.2019-1055

[44] Humphreys, W. M., Jr., Lockard, D. P., Khorrami, M. R., Culliton, W. G., McSwain, R. G., Ravetta, P. A., and Johns, Z., "Development and Calibration of a Field-Deployable Microphone Phased Array for Propulsion and Airframe Noise Flyover Measurements," AIAA Paper 2016-2898, 22nd AIAA/CEAS Aeroacoustics Conference, Lyon, France, 2016. https://doi.org/10.2514/6.2016-2898

[45] Eargle, J., *Loudspeaker Handbook*, 2nd Edition, Kluwer Academic Publishers, 2003. https://doi.org/10.1007/978-1-4757-5678-4

[46] Welch, P.D., "The Use of Fast Fourier Transform for the Estimation of Power Spectra: A Method Based on Time Averaging Over Short Modified Periodograms," IEEE Transactions on Audio and Electroacoustics, Vol. AU-15, pp. 70-73, 1967. https://doi.org/10.1109/TAU.1967.1161901

[47] Dieck, R.H., *Measurement Uncertainty*, 4th Edition, ISA Publishers, 2007.

13.0 Appendices

Appendix A. Array Microphone Design Coordinates for ADL Mockup

Mic #	X Location (in)	Y Location (in)	Z Location (in)	X Location (m)	Y Location (m)	Z Location (m)
1	0.00	0.00	0.00	0.00	0.00	0.00
2	0.00	9.50	0.00	0.00	0.24	0.00
3	-9.50	0.00	0.00	-0.24	0.00	0.00
4	0.00	-9.50	0.00	0.00	-0.24	0.00
5	9.50	0.50	0.00	0.24	0.01	0.00
6	8.30	4.80	0.00	0.21	0.12	0.00
7	4.80	8.30	0.00	0.12	0.21	0.00
8	-4.80	8.30	0.00	-0.12	0.21	0.00
9	-8.30	4.80	0.00	-0.21	0.12	0.00
10	-8.30	-4.80	0.00	-0.21	-0.12	0.00
11	-4.80	-8.30	0.00	-0.12	-0.21	0.00
12	4.80	-8.30	0.00	0.12	-0.21	0.00
13	8.30	-4.80	0.00	0.21	-0.12	0.00
14	13.70	3.70	0.00	0.35	0.09	0.00
15	3.70	13.70	0.00	0.09	0.35	0.00
16	-3.70	13.70	0.00	-0.09	0.35	0.00
17	-13.70	3.70	0.00	-0.35	0.09	0.00
18	-13.70	-3.70	0.00	-0.35	-0.09	0.00
19	-3.70	-13.70	0.00	-0.09	-0.35	0.00
20	3.70	-13.70	0.00	0.09	-0.35	0.00
21	13.70	-3.70	0.00	0.35	-0.09	0.00
22	10.10	10.10	0.00	0.26	0.26	0.00
23	-10.10	10.10	0.00	-0.26	0.26	0.00
24	-10.10	-10.10	0.00	-0.26	-0.26	0.00
25	10.10	-10.10	0.00	0.26	-0.26	0.00
26	8.60	16.80	0.00	0.22	0.43	0.00
27	-16.80	8.60	0.00	-0.43	0.22	0.00
28	-8.60	-16.80	0.00	-0.22	-0.43	0.00
29	16.80	-8.60	0.00	0.43	-0.22	0.00
30	18.80	2.00	0.00	0.48	0.05	0.00
31	-1.00	18.90	0.00	-0.03	0.48	0.00
32	-18.90	-1.00	0.00	-0.48	-0.03	0.00
33	1.00	-18.90	0.00	0.03	-0.48	0.00
34	15.90	10.30	0.00	0.40	0.26	0.00
35	-10.30	15.90	0.00	-0.26	0.40	0.00
36	-15.90	-10.30	0.00	-0.40	-0.26	0.00
37	10.30	-15.90	0.00	0.26	-0.40	0.00
38	19.00	21.10	0.00	0.48	0.54	0.00
39	-21.10	19.00	0.00	-0.54	0.48	0.00
40	-19.00	-21.10	0.00	-0.48	-0.54	0.00
41	21.10	-19.00	0.00	0.54	-0.48	0.00
42	27.00	8.80	0.00	0.69	0.22	0.00

Appendix A. Array Microphone Design Coordinates for ADL Mockup (continued)

Mic #	X Location (in)	Y Location (in)	Z Location (in)	X Location (m)	Y Location (m)	Z Location (m)
43	-8.80	27.00	0.00	-0.22	0.69	0.00
44	-27.00	-8.80	0.00	-0.69	-0.22	0.00
45	8.80	-27.00	0.00	0.22	-0.69	0.00
46	5.90	27.80	0.00	0.15	0.71	0.00
47	-27.80	5.90	0.00	-0.71	0.15	0.00
48	-5.90	-27.80	0.00	-0.15	-0.71	0.00
49	27.80	-5.90	0.00	0.71	-0.15	0.00
50	-61.16	12.98	0.00	-1.55	0.33	0.00
51	-77.84	16.52	0.00	-1.98	0.42	0.00
52	-97.30	20.65	0.00	-2.47	0.52	0.00
53	-116.76	24.78	0.00	-2.97	0.63	0.00
54	-139.00	29.50	0.00	-3.53	0.75	0.00
55	-67.20	34.40	0.00	-1.71	0.87	0.00
56	-92.40	47.30	0.00	-2.35	1.20	0.00
57	-117.60	60.20	0.00	-2.99	1.53	0.00
58	-134.40	68.80	0.00	-3.41	1.75	0.00
59	-46.82	42.16	0.00	-1.19	1.07	0.00
60	-59.08	53.20	0.00	-1.50	1.35	0.00
61	-73.85	66.50	0.00	-1.88	1.69	0.00
62	-88.62	79.80	0.00	-2.25	2.03	0.00
63	-105.50	95.00	0.00	-2.68	2.41	0.00
64	0.00	0.00	0.00	0.00	0.00	0.00
65	-127.07	114.43	0.00	-3.23	2.91	0.00
66	-40.78	62.95	0.00	-1.04	1.60	0.00
67	-56.65	87.45	0.00	-1.44	2.22	0.00
68	-71.77	110.79	0.00	-1.82	2.81	0.00
69	-82.10	126.73	0.00	-2.09	3.22	0.00
70	-92.43	142.68	0.00	-2.35	3.62	0.00
71	-19.52	59.90	0.00	-0.50	1.52	0.00
72	-24.64	75.60	0.00	-0.63	1.92	0.00
73	-30.80	94.50	0.00	-0.78	2.40	0.00
74	-36.96	113.40	0.00	-0.94	2.88	0.00
75	-44.00	135.00	0.00	-1.12	3.43	0.00
76	-3.96	74.90	0.00	-0.10	1.90	0.00
77	-5.50	103.95	0.00	-0.14	2.64	0.00
78	-7.00	132.30	0.00	-0.18	3.36	0.00
79	12.98	61.16	0.00	0.33	1.55	0.00
80	16.52	77.84	0.00	0.42	1.98	0.00
81	20.65	97.30	0.00	0.52	2.47	0.00
82	24.78	116.76	0.00	0.63	2.97	0.00
83	29.50	139.00	0.00	0.75	3.53	0.00
84	34.40	67.20	0.00	0.87	1.71	0.00

Appendix A. Array Microphone Design Coordinates for ADL Mockup (continued)

Mic #	X Location (in)	Y Location (in)	Z Location (in)	X Location (m)	Y Location (m)	Z Location (m)
85	47.30	92.40	0.00	1.20	2.35	0.00
86	60.20	117.60	0.00	1.53	2.99	0.00
87	68.80	134.40	0.00	1.75	3.41	0.00
88	42.16	46.82	0.00	1.07	1.19	0.00
89	53.20	59.08	0.00	1.35	1.50	0.00
90	66.50	73.85	0.00	1.69	1.88	0.00
91	79.80	88.62	0.00	2.03	2.25	0.00
92	95.00	105.50	0.00	2.41	2.68	0.00
93	114.43	127.07	0.00	2.91	3.23	0.00
94	62.95	40.78	0.00	1.60	1.04	0.00
95	87.45	56.65	0.00	2.22	1.44	0.00
96	110.79	71.77	0.00	2.81	1.82	0.00
97	126.73	82.10	0.00	3.22	2.09	0.00
98	142.68	92.43	0.00	3.62	2.35	0.00
99	59.90	19.52	0.00	1.52	0.50	0.00
100	75.60	24.64	0.00	1.92	0.63	0.00
101	94.50	30.80	0.00	2.40	0.78	0.00
102	113.40	36.96	0.00	2.88	0.94	0.00
103	135.00	44.00	0.00	3.43	1.12	0.00
104	74.58	7.93	0.00	1.89	0.20	0.00
105	103.40	11.00	0.00	2.63	0.28	0.00
106	131.60	14.00	0.00	3.34	0.36	0.00
107	61.16	-12.98	0.00	1.55	-0.33	0.00
108	77.84	-16.52	0.00	1.98	-0.42	0.00
109	97.30	-20.65	0.00	2.47	-0.52	0.00
110	116.76	-24.78	0.00	2.97	-0.63	0.00
111	139.00	-29.50	0.00	3.53	-0.75	0.00
112	67.20	-34.40	0.00	1.71	-0.87	0.00
113	92.40	-47.30	0.00	2.35	-1.20	0.00
114	134.40	-68.80	0.00	3.41	-1.75	0.00
115	117.60	-60.20	0.00	2.99	-1.53	0.00
116	46.82	-42.16	0.00	1.19	-1.07	0.00
117	59.08	-53.20	0.00	1.50	-1.35	0.00
118	73.85	-66.50	0.00	1.88	-1.69	0.00
119	88.62	-79.80	0.00	2.25	-2.03	0.00
120	105.50	-95.00	0.00	2.68	-2.41	0.00
121	127.07	-114.43	0.00	3.23	-2.91	0.00
122	40.78	-62.95	0.00	1.04	-1.60	0.00
123	56.65	-87.45	0.00	1.44	-2.22	0.00
124	71.77	-110.79	0.00	1.82	-2.81	0.00

Appendix A. Array Microphone Design Coordinates for ADL Mockup (concluded)

Mic #	X Location (in)	Y Location (in)	Z Location (in)	X Location (m)	Y Location (m)	Z Location (m)
125	82.10	-126.73	0.00	2.09	-3.22	0.00
126	92.43	-142.68	0.00	2.35	-3.62	0.00
127	19.52	-59.90	0.00	0.50	-1.52	0.00
128	0.00	0.00	0.00	0.00	0.00	0.00
129	24.64	-75.60	0.00	0.63	-1.92	0.00
130	30.80	-94.50	0.00	0.78	-2.40	0.00
131	36.96	-113.40	0.00	0.94	-2.88	0.00
132	44.00	-135.00	0.00	1.12	-3.43	0.00
133	3.96	-74.90	0.00	0.10	-1.90	0.00
134	5.50	-103.95	0.00	0.14	-2.64	0.00
135	7.00	-132.30	0.00	0.18	-3.36	0.00
136	-12.98	-61.16	0.00	-0.33	-1.55	0.00
137	-16.52	-77.84	0.00	-0.42	-1.98	0.00
138	-20.65	-97.30	0.00	-0.52	-2.47	0.00
139	-24.78	-116.76	0.00	-0.63	-2.97	0.00
140	-29.50	-139.00	0.00	-0.75	-3.53	0.00
141	-34.40	-67.20	0.00	-0.87	-1.71	0.00
142	-47.30	-92.40	0.00	-1.20	-2.35	0.00
143	-60.20	-117.60	0.00	-1.53	-2.99	0.00
144	-68.80	-134.40	0.00	-1.75	-3.41	0.00
145	-42.16	-46.82	0.00	-1.07	-1.19	0.00
146	-53.20	-59.08	0.00	-1.35	-1.50	0.00
147	-66.50	-73.85	0.00	-1.69	-1.88	0.00
148	-79.80	-88.62	0.00	-2.03	-2.25	0.00
149	-95.00	-105.50	0.00	-2.41	-2.68	0.00
150	-114.43	-127.07	0.00	-2.91	-3.23	0.00
151	-62.95	-40.78	0.00	-1.60	-1.04	0.00
152	-87.45	-56.65	0.00	-2.22	-1.44	0.00
153	-110.79	-71.77	0.00	-2.81	-1.82	0.00
154	-126.73	-82.10	0.00	-3.22	-2.09	0.00
155	-142.68	-92.43	0.00	-3.62	-2.35	0.00
156	-59.90	-19.52	0.00	-1.52	-0.50	0.00
157	-75.60	-24.64	0.00	-1.92	-0.63	0.00
158	-94.50	-30.80	0.00	-2.40	-0.78	0.00
159	-113.40	-36.96	0.00	-2.88	-0.94	0.00
160	-135.00	-44.00	0.00	-3.43	-1.12	0.00
161	-74.90	-3.96	0.00	-1.90	-0.10	0.00
162	-103.95	-5.50	0.00	-2.64	-0.14	0.00
163	-132.30	-7.00	0.00	-3.36	-0.18	0.00

Note: All coordinates are referenced to the center of the array.

Appendix B. Array Microphone Design Coordinates for Fort A.P. Hill 2015 Deployment

Mic #	X Location (in)	Y Location (in)	Z Location (in)	X Location (m)	Y Location (m)	Z Location (m)
1	0.00	0.00	0.00	0.00	0.00	0.00
2	9.50	0.00	0.00	0.24	0.00	0.00
3	0.00	-9.50	0.00	0.00	-0.24	0.00
4	-9.50	0.00	0.00	-0.24	0.00	0.00
5	0.50	9.50	0.00	0.01	0.24	0.00
6	4.80	8.30	0.00	0.12	0.21	0.00
7	8.30	4.80	0.00	0.21	0.12	0.00
8	8.30	-4.80	0.00	0.21	-0.12	0.00
9	4.80	-8.30	0.00	0.12	-0.21	0.00
10	-4.80	-8.30	0.00	-0.12	-0.21	0.00
11	-8.30	-4.80	0.00	-0.21	-0.12	0.00
12	-8.30	4.80	0.00	-0.21	0.12	0.00
13	-4.80	8.30	0.00	-0.12	0.21	0.00
14	3.70	13.70	0.00	0.09	0.35	0.00
15	13.70	3.70	0.00	0.35	0.09	0.00
16	13.70	-3.70	0.00	0.35	-0.09	0.00
17	3.70	-13.70	0.00	0.09	-0.35	0.00
18	-3.70	-13.70	0.00	-0.09	-0.35	0.00
19	-13.70	-3.70	0.00	-0.35	-0.09	0.00
20	-13.70	3.70	0.00	-0.35	0.09	0.00
21	-3.70	13.70	0.00	-0.09	0.35	0.00
22	10.10	10.10	0.00	0.26	0.26	0.00
23	10.10	-10.10	0.00	0.26	-0.26	0.00
24	-10.10	-10.10	0.00	-0.26	-0.26	0.00
25	-10.10	10.10	0.00	-0.26	0.26	0.00
26	16.80	8.60	0.00	0.43	0.22	0.00
27	8.60	-16.80	0.00	0.22	-0.43	0.00
28	-16.80	-8.60	0.00	-0.43	-0.22	0.00
29	-8.60	16.80	0.00	-0.22	0.43	0.00
30	2.00	18.80	0.00	0.05	0.48	0.00
31	18.90	-1.00	0.00	0.48	-0.03	0.00
32	-1.00	-18.90	0.00	-0.03	-0.48	0.00
33	-18.90	1.00	0.00	-0.48	0.03	0.00
34	10.30	15.90	0.00	0.26	0.40	0.00
35	15.90	-10.30	0.00	0.40	-0.26	0.00
36	-10.30	-15.90	0.00	-0.26	-0.40	0.00
37	-15.90	10.30	0.00	-0.40	0.26	0.00
38	21.10	19.00	0.00	0.54	0.48	0.00
39	19.00	-21.10	0.00	0.48	-0.54	0.00
40	-21.10	-19.00	0.00	-0.54	-0.48	0.00
41	-19.00	21.10	0.00	-0.48	0.54	0.00
42	8.80	27.00	0.00	0.22	0.69	0.00

Appendix B. Array Microphone Design Coordinates for Fort A.P. Hill 2015 Deployment (continued)

Mic #	X Location (in)	Y Location (in)	Z Location (in)	X Location (m)	Y Location (m)	Z Location (m)
43	27.00	-8.80	0.00	0.69	-0.22	0.00
44	-8.80	-27.00	0.00	-0.22	-0.69	0.00
45	-27.00	8.80	0.00	-0.69	0.22	0.00
46	27.80	5.90	0.00	0.71	0.15	0.00
47	5.90	-27.80	0.00	0.15	-0.71	0.00
48	-27.80	-5.90	0.00	-0.71	-0.15	0.00
49	-5.90	27.80	0.00	-0.15	0.71	0.00
50	-87.00	-26.72	0.00	-2.21	-0.68	0.00
51	-111.69	-32.43	0.00	-2.84	-0.82	0.00
52	-139.93	-46.29	0.00	-3.55	-1.18	0.00
53	-171.47	-45.94	0.00	-4.36	-1.17	0.00
54	-200.99	-62.78	0.00	-5.11	-1.59	0.00
55	-239.91	-71.90	0.00	-6.09	-1.83	0.00
56	-281.65	-91.78	0.00	-7.15	-2.33	0.00
57	-333.92	-109.83	0.00	-8.48	-2.79	0.00
58	-399.94	-121.58	0.00	-10.16	-3.09	0.00
59	-468.37	-151.83	0.00	-11.90	-3.86	0.00
60	-551.49	-173.70	0.00	-14.01	-4.41	0.00
61	-64.43	-63.51	0.00	-1.64	-1.61	0.00
62	-87.67	-76.76	0.00	-2.23	-1.95	0.00
63	-106.03	-101.39	0.00	-2.69	-2.58	0.00
64	-132.23	-117.20	0.00	-3.36	-2.98	0.00
65	-147.74	-151.79	0.00	-3.75	-3.86	0.00
66	-185.17	-168.46	0.00	-4.70	-4.28	0.00
67	-210.23	-212.88	0.00	-5.34	-5.41	0.00
68	-260.08	-237.22	0.00	-6.61	-6.03	0.00
69	-296.05	-290.99	0.00	-7.52	-7.39	0.00
70	-359.41	-333.45	0.00	-9.13	-8.47	0.00
71	-415.83	-401.96	0.00	-10.56	-10.21	0.00
72	-501.64	-476.46	0.00	-12.74	-12.10	0.00
73	-24.57	-87.68	0.00	-0.62	-2.23	0.00
74	-28.33	-112.36	0.00	-0.72	-2.85	0.00
75	-42.09	-140.29	0.00	-1.07	-3.56	0.00
76	-39.78	-172.11	0.00	-1.01	-4.37	0.00
77	-57.25	-203.19	0.00	-1.45	-5.16	0.00
78	-53.27	-245.80	0.00	-1.35	-6.24	0.00
79	-79.29	-287.32	0.00	-2.01	-7.30	0.00
80	-77.55	-343.09	0.00	-1.97	-8.71	0.00
81	-107.66	-402.59	0.00	-2.73	-10.23	0.00
82	-119.26	-476.20	0.00	-3.03	-12.10	0.00
83	-129.14	-219.18	0.00	-3.28	-5.57	0.00
84	30.21	-86.34	0.00	0.77	-2.19	0.00

Appendix B. Array Microphone Design Coordinates for Fort A.P. Hill 2015 Deployment (continued)

Mic #	X Location (in)	Y Location (in)	Z Location (in)	X Location (m)	Y Location (m)	Z Location (m)
85	26.44	-114.01	0.00	0.67	-2.90	0.00
86	48.69	-140.02	0.00	1.24	-3.56	0.00
87	42.56	-172.77	0.00	1.08	-4.39	0.00
88	65.38	-201.84	0.00	1.66	-5.13	0.00
89	63.86	-244.45	0.00	1.62	-6.21	0.00
90	89.49	-284.18	0.00	2.27	-7.22	0.00
91	90.47	-341.37	0.00	2.30	-8.67	0.00
92	109.66	-401.90	0.00	2.79	-10.21	0.00
93	137.03	-471.81	0.00	3.48	-11.98	0.00
94	-2.29	-199.98	0.00	-0.06	-5.08	0.00
95	62.74	-67.21	0.00	1.59	-1.71	0.00
96	87.23	-78.65	0.00	2.22	-2.00	0.00
97	101.80	-108.36	0.00	2.59	-2.75	0.00
98	130.68	-119.68	0.00	3.32	-3.04	0.00
99	147.27	-154.49	0.00	3.74	-3.92	0.00
100	184.32	-173.05	0.00	4.68	-4.40	0.00
101	209.38	-214.69	0.00	5.32	-5.45	0.00
102	257.55	-243.50	0.00	6.54	-6.19	0.00
103	290.99	-297.81	0.00	7.39	-7.56	0.00
104	354.62	-341.17	0.00	9.01	-8.67	0.00
105	413.50	-408.20	0.00	10.50	-10.37	0.00
106	124.90	-202.65	0.00	3.17	-5.15	0.00
107	92.16	-14.15	0.00	2.34	-0.36	0.00
108	111.90	-33.47	0.00	2.84	-0.85	0.00
109	146.35	-24.93	0.00	3.72	-0.63	0.00
110	173.00	-41.53	0.00	4.39	-1.05	0.00
111	206.02	-55.53	0.00	5.23	-1.41	0.00
112	247.27	-52.60	0.00	6.28	-1.34	0.00
113	289.27	-75.93	0.00	7.35	-1.93	0.00
114	345.25	-76.21	0.00	8.77	-1.94	0.00
115	402.62	-103.74	0.00	10.23	-2.64	0.00
116	480.49	-107.66	0.00	12.20	-2.73	0.00
117	561.93	-142.31	0.00	14.27	-3.61	0.00
118	88.41	23.67	0.00	2.25	0.60	0.00
119	110.57	39.92	0.00	2.81	1.01	0.00
120	143.03	38.38	0.00	3.63	0.97	0.00
121	167.30	60.93	0.00	4.25	1.55	0.00
122	202.35	59.46	0.00	5.14	1.51	0.00
123	239.61	80.67	0.00	6.09	2.05	0.00
124	287.35	84.69	0.00	7.30	2.15	0.00
125	334.03	116.22	0.00	8.48	2.95	0.00
126	399.56	122.01	0.00	10.15	3.10	0.00

Appendix B. Array Microphone Design Coordinates for Fort A.P. Hill 2015 Deployment (continued)

Mic #	X Location (in)	Y Location (in)	Z Location (in)	X Location (m)	Y Location (m)	Z Location (m)
127	466.36	158.87	0.00	11.85	4.04	0.00
128	555.61	172.78	0.00	14.11	4.39	0.00
129	62.62	68.03	0.00	1.59	1.73	0.00
130	85.28	81.67	0.00	2.17	2.07	0.00
131	97.09	112.70	0.00	2.47	2.86	0.00
132	132.13	122.76	0.00	3.36	3.12	0.00
133	140.35	160.97	0.00	3.56	4.09	0.00
134	177.95	180.87	0.00	4.52	4.59	0.00
135	199.57	223.19	0.00	5.07	5.67	0.00
136	247.06	253.74	0.00	6.28	6.44	0.00
137	281.06	308.44	0.00	7.14	7.83	0.00
138	340.55	355.36	0.00	8.65	9.03	0.00
139	393.70	426.70	0.00	10.00	10.84	0.00
140	451.44	472.30	0.00	11.47	12.00	0.00
141	14.54	92.07	0.00	0.37	2.34	0.00
142	32.28	111.08	0.00	0.82	2.82	0.00
143	26.23	145.99	0.00	0.67	3.71	0.00
144	45.36	171.45	0.00	1.15	4.35	0.00
145	40.59	208.99	0.00	1.03	5.31	0.00
146	62.53	245.02	0.00	1.59	6.22	0.00
147	60.15	293.44	0.00	1.53	7.45	0.00
148	84.68	342.06	0.00	2.15	8.69	0.00
149	85.99	407.29	0.00	2.18	10.35	0.00
150	108.88	448.38	0.00	2.77	11.39	0.00
151	110.24	206.52	0.00	2.80	5.25	0.00
152	-24.08	84.46	0.00	-0.61	2.15	0.00
153	-40.97	111.69	0.00	-1.04	2.84	0.00
154	-37.76	142.37	0.00	-0.96	3.62	0.00
155	-58.95	168.26	0.00	-1.50	4.27	0.00
156	-59.21	204.92	0.00	-1.50	5.20	0.00
157	-80.77	240.61	0.00	-2.05	6.11	0.00
158	-85.46	285.18	0.00	-2.17	7.24	0.00
159	-111.37	334.59	0.00	-2.83	8.50	0.00
160	-119.50	397.50	0.00	-3.04	10.10	0.00
161	-141.74	434.75	0.00	-3.60	11.04	0.00
162	-14.59	268.93	0.00	-0.37	6.83	0.00
163	-63.93	66.04	0.00	-1.62	1.68	0.00
164	-88.04	78.42	0.00	-2.24	1.99	0.00
165	-103.47	106.48	0.00	-2.63	2.70	0.00
166	-133.57	118.57	0.00	-3.39	3.01	0.00

Appendix B. Array Microphone Design Coordinates for Fort A.P. Hill 2015 Deployment (concluded)

Mic #	X Location (in)	Y Location (in)	Z Location (in)	X Location (m)	Y Location (m)	Z Location (m)
167	-149.21	150.09	0.00	-3.79	3.81	0.00
168	-184.76	171.37	0.00	-4.69	4.35	0.00
169	-210.30	207.87	0.00	-5.34	5.28	0.00
170	-261.51	240.05	0.00	-6.64	6.10	0.00
171	-296.69	292.67	0.00	-7.54	7.43	0.00
172	-363.02	334.78	0.00	-9.22	8.50	0.00
173	-421.38	399.06	0.00	-10.70	10.14	0.00
174	-295.46	187.50	0.00	-7.50	4.76	0.00
175	-86.21	24.86	0.00	-2.19	0.63	0.00
176	-113.69	21.78	0.00	-2.89	0.55	0.00
177	-139.40	39.26	0.00	-3.54	1.00	0.00
178	-172.63	35.17	0.00	-4.38	0.89	0.00
179	-204.18	53.83	0.00	-5.19	1.37	0.00
180	-241.43	62.46	0.00	-6.13	1.59	0.00
181	-286.48	73.33	0.00	-7.28	1.86	0.00
182	-347.60	72.80	0.00	-8.83	1.85	0.00
183	-405.65	87.62	0.00	-10.30	2.23	0.00
184	-478.56	100.95	0.00	-12.16	2.56	0.00
185	-562.17	139.99	0.00	-14.28	3.56	0.00

Note: All coordinates are referenced to the center of the array.

Appendix C. Array Microphone Design Coordinates for Edwards AFB Deployments

Mic #	X Location (in)	Y Location (in)	Z Location (in)	X Location (m)	Y Location (m)	Z Location (m)
1	0.00	0.00	0.00	0.00	0.00	0.00
2	0.00	-9.50	0.00	0.00	-0.24	0.00
3	-9.50	0.00	0.00	-0.24	0.00	0.00
4	0.00	9.50	0.00	0.00	0.24	0.00
5	9.50	-0.50	0.00	0.24	-0.01	0.00
6	8.30	-4.79	0.00	0.21	-0.12	0.00
7	4.79	-8.30	0.00	0.12	-0.21	0.00
8	-4.79	-8.30	0.00	-0.12	-0.21	0.00
9	-8.30	-4.79	0.00	-0.21	-0.12	0.00
10	-8.30	4.79	0.00	-0.21	0.12	0.00
11	-4.79	8.30	0.00	-0.12	0.21	0.00
12	4.79	8.30	0.00	0.12	0.21	0.00
13	8.30	4.79	0.00	0.21	0.12	0.00
14	13.70	-3.70	0.00	0.35	-0.09	0.00
15	3.70	-13.70	0.00	0.09	-0.35	0.00
16	-3.70	-13.70	0.00	-0.09	-0.35	0.00
17	-13.70	-3.70	0.00	-0.35	-0.09	0.00
18	-13.70	3.70	0.00	-0.35	0.09	0.00
19	-3.70	13.70	0.00	-0.09	0.35	0.00
20	3.70	13.70	0.00	0.09	0.35	0.00
21	13.70	3.70	0.00	0.35	0.09	0.00
22	10.10	-10.10	0.00	0.26	-0.26	0.00
23	-10.10	-10.10	0.00	-0.26	-0.26	0.00
24	-10.10	10.10	0.00	-0.26	0.26	0.00
25	10.10	10.10	0.00	0.26	0.26	0.00
26	8.60	-16.80	0.00	0.22	-0.43	0.00
27	-16.80	-8.60	0.00	-0.43	-0.22	0.00
28	-8.60	16.80	0.00	-0.22	0.43	0.00
29	16.80	8.60	0.00	0.43	0.22	0.00
30	18.80	-2.01	0.00	0.48	-0.05	0.00
31	-0.99	-18.90	0.00	-0.03	-0.48	0.00
32	-18.90	0.99	0.00	-0.48	0.03	0.00
33	0.99	18.90	0.00	0.03	0.48	0.00
34	15.91	-10.29	0.00	0.40	-0.26	0.00
35	-10.29	-15.91	0.00	-0.26	-0.40	0.00
36	-15.91	10.29	0.00	-0.40	0.26	0.00
37	10.29	15.91	0.00	0.26	0.40	0.00
38	19.00	-21.10	0.00	0.48	-0.54	0.00
39	-21.10	-19.00	0.00	-0.54	-0.48	0.00
40	-19.00	21.10	0.00	-0.48	0.54	0.00
41	21.10	19.00	0.00	0.54	0.48	0.00
42	26.99	-8.82	0.00	0.69	-0.22	0.00

Appendix C. Array Microphone Design Coordinates for Edwards AFB Deployments (continued)

Mic #	X Location (in)	Y Location (in)	Z Location (in)	X Location (m)	Y Location (m)	Z Location (m)
43	-8.82	-26.99	0.00	-0.22	-0.69	0.00
44	-26.99	8.82	0.00	-0.69	0.22	0.00
45	8.82	26.99	0.00	0.22	0.69	0.00
46	5.91	-27.80	0.00	0.15	-0.71	0.00
47	-27.80	-5.91	0.00	-0.71	-0.15	0.00
48	-5.91	27.80	0.00	-0.15	0.71	0.00
49	27.80	5.91	0.00	0.71	0.15	0.00
50	-76.50	-23.39	0.00	-1.94	-0.59	0.00
51	-133.65	-68.10	0.00	-3.39	-1.73	0.00
52	-199.29	-124.53	0.00	-5.06	-3.16	0.00
53	-234.80	-176.93	0.00	-5.96	-4.49	0.00
54	-272.73	-245.57	0.00	-6.93	-6.24	0.00
55	-313.04	-335.69	0.00	-7.95	-8.53	0.00
56	-352.77	-451.53	0.00	-8.96	-11.47	0.00
57	-390.51	-601.33	0.00	-9.92	-15.27	0.00
58	-420.65	-791.12	0.00	-10.68	-20.09	0.00
59	-437.62	-1030.97	0.00	-11.12	-26.19	0.00
60	-463.52	-1426.59	0.00	-11.77	-36.24	0.00
61	-54.56	-58.51	0.00	-1.39	-1.49	0.00
62	-92.35	-118.20	0.00	-2.35	-3.00	0.00
63	-102.39	-157.67	0.00	-2.60	-4.00	0.00
64	-110.33	-207.49	0.00	-2.80	-5.27	0.00
65	-114.87	-270.63	0.00	-2.92	-6.87	0.00
66	-113.41	-349.04	0.00	-2.88	-8.87	0.00
67	-103.25	-447.24	0.00	-2.62	-11.36	0.00
68	-79.75	-567.42	0.00	-2.03	-14.41	0.00
69	-37.52	-716.02	0.00	-0.95	-18.19	0.00
70	31.27	-895.45	0.00	0.79	-22.74	0.00
71	136.50	-1111.65	0.00	3.47	-28.24	0.00
72	311.87	-1467.22	0.00	7.92	-37.27	0.00
73	-18.00	-77.95	0.00	-0.46	-1.98	0.00
74	-7.85	-149.79	0.00	-0.20	-3.80	0.00
75	8.20	-234.86	0.00	0.21	-5.97	0.00
76	35.83	-291.81	0.00	0.91	-7.41	0.00
77	76.30	-358.98	0.00	1.94	-9.12	0.00
78	134.20	-438.94	0.00	3.41	-11.15	0.00
79	214.65	-531.28	0.00	5.45	-13.49	0.00
80	325.51	-638.85	0.00	8.27	-16.23	0.00
81	474.81	-759.85	0.00	12.06	-19.30	0.00
82	674.03	-894.47	0.00	17.12	-22.72	0.00
83	936.78	-1040.40	0.00	23.79	-26.43	0.00

Appendix C. Array Microphone Design Coordinates for Edwards AFB Deployments (continued)

Mic #	X Location (in)	Y Location (in)	Z Location (in)	X Location (m)	Y Location (m)	Z Location (m)
84	23.39	-76.50	0.00	0.59	-1.94	0.00
85	68.10	-133.65	0.00	1.73	-3.39	0.00
86	124.53	-199.29	0.00	3.16	-5.06	0.00
87	176.93	-234.80	0.00	4.49	-5.96	0.00
88	245.57	-272.73	0.00	6.24	-6.93	0.00
89	335.69	-313.04	0.00	8.53	-7.95	0.00
90	451.53	-352.77	0.00	11.47	-8.96	0.00
91	601.33	-390.51	0.00	15.27	-9.92	0.00
92	791.12	-420.65	0.00	20.09	-10.68	0.00
93	1030.97	-437.62	0.00	26.19	-11.12	0.00
94	1426.58	-463.53	0.00	36.24	-11.77	0.00
95	58.51	-54.56	0.00	1.49	-1.39	0.00
96	118.20	-92.35	0.00	3.00	-2.35	0.00
97	157.67	-102.39	0.00	4.00	-2.60	0.00
98	207.49	-110.33	0.00	5.27	-2.80	0.00
99	270.63	-114.87	0.00	6.87	-2.92	0.00
100	349.04	-113.41	0.00	8.87	-2.88	0.00
101	447.24	-103.25	0.00	11.36	-2.62	0.00
102	567.42	-79.75	0.00	14.41	-2.03	0.00
103	716.02	-37.52	0.00	18.19	-0.95	0.00
104	895.45	31.27	0.00	22.74	0.79	0.00
105	1111.65	136.49	0.00	28.24	3.47	0.00
106	1467.22	311.87	0.00	37.27	7.92	0.00
107	77.95	-18.00	0.00	1.98	-0.46	0.00
108	149.79	-7.85	0.00	3.80	-0.20	0.00
109	234.86	8.20	0.00	5.97	0.21	0.00
110	291.81	35.83	0.00	7.41	0.91	0.00
111	358.98	76.30	0.00	9.12	1.94	0.00
112	438.94	134.20	0.00	11.15	3.41	0.00
113	531.28	214.65	0.00	13.49	5.45	0.00
114	638.85	325.51	0.00	16.23	8.27	0.00
115	759.85	474.81	0.00	19.30	12.06	0.00
116	894.47	674.03	0.00	22.72	17.12	0.00
117	1114.72	1003.70	0.00	28.31	25.49	0.00
118	76.50	23.39	0.00	1.94	0.59	0.00
119	133.65	68.10	0.00	3.39	1.73	0.00
120	199.29	124.53	0.00	5.06	3.16	0.00
121	234.80	176.93	0.00	5.96	4.49	0.00
122	272.73	245.57	0.00	6.93	6.24	0.00
123	313.04	335.69	0.00	7.95	8.53	0.00
124	352.77	451.53	0.00	8.96	11.47	0.00
125	390.51	601.33	0.00	9.92	15.27	0.00

Appendix C. Array Microphone Design Coordinates for Edwards AFB Deployments (continued)

Mic #	X Location (in)	Y Location (in)	Z Location (in)	X Location (m)	Y Location (m)	Z Location (m)
126	420.65	791.12	0.00	10.68	20.09	0.00
127	437.62	1030.97	0.00	11.12	26.19	0.00
128	463.53	1426.58	0.00	11.77	36.24	0.00
129	54.56	58.51	0.00	1.39	1.49	0.00
130	92.35	118.20	0.00	2.35	3.00	0.00
131	102.39	157.67	0.00	2.60	4.00	0.00
132	110.33	207.49	0.00	2.80	5.27	0.00
133	114.88	270.63	0.00	2.92	6.87	0.00
134	113.41	349.04	0.00	2.88	8.87	0.00
135	103.25	447.24	0.00	2.62	11.36	0.00
136	79.75	567.42	0.00	2.03	14.41	0.00
137	37.53	716.02	0.00	0.95	18.19	0.00
138	-31.27	895.45	0.00	-0.79	22.74	0.00
139	-136.49	1111.65	0.00	-3.47	28.24	0.00
140	-311.87	1467.22	0.00	-7.92	37.27	0.00
141	18.00	77.95	0.00	0.46	1.98	0.00
142	7.85	149.79	0.00	0.20	3.80	0.00
143	-8.20	234.86	0.00	-0.21	5.97	0.00
144	-35.83	291.81	0.00	-0.91	7.41	0.00
145	-76.30	358.98	0.00	-1.94	9.12	0.00
146	-134.20	438.94	0.00	-3.41	11.15	0.00
147	-214.65	531.28	0.00	-5.45	13.49	0.00
148	-325.51	638.85	0.00	-8.27	16.23	0.00
149	-474.81	759.85	0.00	-12.06	19.30	0.00
150	-674.03	894.47	0.00	-17.12	22.72	0.00
151	-1003.69	1114.72	0.00	-25.49	28.31	0.00
152	-23.39	76.50	0.00	-0.59	1.94	0.00
153	-68.10	133.65	0.00	-1.73	3.39	0.00
154	-124.53	199.29	0.00	-3.16	5.06	0.00
155	-176.93	234.80	0.00	-4.49	5.96	0.00
156	-245.57	272.73	0.00	-6.24	6.93	0.00
157	-335.69	313.04	0.00	-8.53	7.95	0.00
158	-451.53	352.77	0.00	-11.47	8.96	0.00
159	-601.33	390.51	0.00	-15.27	9.92	0.00
160	-791.12	420.65	0.00	-20.09	10.68	0.00
161	-1030.96	437.62	0.00	-26.19	11.12	0.00
162	-1426.58	463.53	0.00	-36.24	11.77	0.00
163	-58.51	54.56	0.00	-1.49	1.39	0.00
164	-118.20	92.35	0.00	-3.00	2.35	0.00
165	-157.67	102.39	0.00	-4.00	2.60	0.00
166	-207.49	110.33	0.00	-5.27	2.80	0.00

Appendix C. Array Microphone Design Coordinates for Edwards AFB Deployments (concluded)

Mic #	X Location (in)	Y Location (in)	Z Location (in)	X Location (m)	Y Location (m)	Z Location (m)
167	-270.63	114.88	0.00	-6.87	2.92	0.00
168	-349.04	113.41	0.00	-8.87	2.88	0.00
169	-447.24	103.25	0.00	-11.36	2.62	0.00
170	-567.42	79.75	0.00	-14.41	2.03	0.00
171	-716.02	37.53	0.00	-18.19	0.95	0.00
172	-895.45	-31.27	0.00	-22.74	-0.79	0.00
173	-1111.65	-136.49	0.00	-28.24	-3.47	0.00
174	-1467.22	-311.86	0.00	-37.27	-7.92	0.00
175	-77.95	18.00	0.00	-1.98	0.46	0.00
176	-149.79	7.85	0.00	-3.80	0.20	0.00
177	-234.86	-8.20	0.00	-5.97	-0.21	0.00
178	-291.81	-35.83	0.00	-7.41	-0.91	0.00
179	-358.98	-76.30	0.00	-9.12	-1.94	0.00
180	-438.94	-134.20	0.00	-11.15	-3.41	0.00
181	-531.28	-214.65	0.00	-13.49	-5.45	0.00
182	-638.85	-325.51	0.00	-16.23	-8.27	0.00
183	-759.85	-474.81	0.00	-19.30	-12.06	0.00
184	-894.47	-674.03	0.00	-22.72	-17.12	0.00
185	-1114.72	-1003.69	0.00	-28.31	-25.49	0.00

Note: All coordinates are referenced to the center of the array.